Studies of nano-photonic quantum emitter arrays using generalized mean field methods

Maxim Laborenz, B.Sc.

February 25, 2024

Masterarbeit
zur Erlangung des akademischen Grades
Master of Science, Physik

eingereicht an der
Fakultät für Mathematik, Informatik und Physik
der Leopold-Franzens-Universität Innsbruck

Betreuer:
Dr. Laurin Ostermann
Univ.-Prof. Dr. Helmut Ritsch

universität innsbruck

Kurzfassung

Diese Masterarbeit widmet sich der Untersuchung der Gültigkeit der Kumulanten Entwicklung, welche ursprünglich von Kubo im Jahre 1962 als Näherungsmethode konzipiert wurde, mittels derer man Korrelationen zwischen statistischen Variablen bis zu einer gewünschten Ordnung entfernt, was zu weniger Rechenzeit führt. Allerdings auf Kosten der exakten Lösung, was den Verlust von quantenphysikalischen Eigenschaften wie Verschränkung oder Super- & Subradianz bedeuten kann. Die Kumulanten Entwicklung wird sich als effizientes Werkzeug im Umgang mit komplexen Quantenphänomenen herausstellen.

Weiterhin finden wir jenseits seiner Bedeutung als Näherungsmethode, dass der Vergleich zwischen verschiedenen Ordnungen womöglich für Experimente interessante Parameterbereiche aufdecken und beim Ausloten der Grenzen zwischen klassischer und Quantenphysik behilflich sein kann.

Diese Arbeit trägt hoffentlich dazu bei das Verständnis, die Validität sowie den Nutzungsbereich der Kumulanten Entwicklung zu fördern, zu ergründen und auszuweiten, um ihr den Weg in weitere wissenschaftliche Zweige zu ebnen.

Abstract

This thesis delves into the exploration of the validity and expansion of the cumulant expansion, a mathematical tool introduced by Kubo in 1962 in order to eliminate correlations between statistical variables beyond a desired order to simplify calculations, yielding faster computation time at the cost of the exact solution, which can mean losing quantum physics such like entanglement or super- & subradiance. The cumulant expansion will emerge as a computationally efficient approach, showcasing remarkable performance in handling complex quantum phenomena.

Notably, our research reveals that the cumulant expansion transcends its conventional role. Beyond mere computational utility, we leverage its application by comparing different orders, offering insights into parameter regimes of interest. This comparison becomes crucial in clarifying the boundaries between classical and quantum physics. In doing so, we extend the scope of the cumulant expansion.

This thesis contributes to a deeper understanding of the cumulant expansion's capabilities and broadens its application, paving the way for enhanced insights across various scientific domains.

Contents

1 Introduction

Light is easily one of the most important constituents of the physics of our world. Our eyesight fully depends on it, making it one of the oldest topics in physics. Euclid for example treated perspective already[1] and even in ancient china people worked on theories regarding the propagation of light through lenses[2]. Way later, in the 19th century, J. C. Maxwell derived the speed of light in vacuum using his famous formulas, yielding a connection between optics and electrodynamics as he found light to be an electromagnetic wave. Roughly hundred years later N. Bohr expanded our understanding of the origin of light by introducing one of the first quantum models for atoms[3]. He proposed, that electrons in the atom shells can only take discrete rather than continuous energy states and transitions between them appear among other techniques through absorption or emission of the electromagnetic interaction particle, i.e. photons of energy $\hbar\omega$, where ω is the transition frequency between the two states.

Especially interesting in the context of this thesis is the concept of spontaneous emission in open systems. If an atom is not in the ground state, it has a probability to interact with the electromagnetic vacuum and emit a photon into a random direction in order to minimize its own energy, as studied by Einstein with his famous Einstein-coefficients[9]. This leads to an instantaneous jump to a lower energy state at random times. Such transitions are categorized by their transition frequency and the decay rate Γ corresponding to the decay channel.

Every atom eventually undergoes this random process individually. However R. H. Dicke found out, that in addition in the quantum regime, i.e. when atoms are spaced by less than the transition wavelength, identical atoms change to a collective behaviour, showing modified energy levels and decay rates compared to the individual case, resulting in phenomena like the famous Dicke super- and subradiance and superradiant pulses with relevance in biological systems as well [4].

The decay rate Γ_{ij} for the transition from a state i to j, describes the mean time identical atoms in an ensemble need to decay along that channel and is thus a very statistical quantity. Much more the whole quantum theory is a statistical theory and therefore one will often encounter typical statistical approaches like calculating the mean or the expectation value of quantum mechanical operators when treating a problem quantum mechanically.

Another common issue apart of the statistical nature of quantum mechanics is that the Hilbert space of a problem and thus its complexity grows exponentially.

For example in the case of N two-level emitters the describing state vector grows with 2^N and thus operators, which are represented by matrices, with $2^N \times 2^N$[5], quickly lead to untreatable systems. Realistic biological systems e.g. with hundreds of atoms involved are barely treatable and need computers to work for years.

The only way to grant access to such systems without using more capable computers, is approximating results. For higher order bosonic annihilation/creation operator correlation functions one can e.g. use Wick's theorem[6] and express the product by taking all contractions. Another approach capable of treating less restricted quantities is applying the widely used mean-field approximation, which uncorrelates two statistical quantities A and B such that the expectation value of the product is simplified to be $\langle AB\rangle \approx \langle A\rangle\langle B\rangle$. One can extend the expansion theory for higher order products and regard the mean-field approximation as the lowest order case of the "cumulant expansion", introduced by Ryogo Kubo in 1962 [7], who was first to generalize it so the considered stochastic variables don't need to be ordinary c-numbers but may be quantum mechanical operators instead, making it useful for equations containing such operators.
Since quantum theory is a stochastic theory, cumulants play a key-role as they determine probability distributions. The cumulant expansion turns out to be a very mighty tool to approximate not just quantum, but all kinds of dynamics where statistical fluctuations are present.
In the context of quantum physics, and in this thesis specifically quantum optics, its usage allows to neglect quantum correlations beyond a desired order, making underlying ordinary differential equation systems tractable. The complexity of problems then scales polynomially rather than exponentially [5]. In our case this grants access to simulations of large arrays of quantum emitters and studies on their quantum optical properties.

However it remains an approximation method for which the convergence towards the correct result is not mathematically proven yet, but due to its universality it is definitely worth looking into its performance, its limitations and its further usage. To this end this thesis seeks to motivate the usage of the cumulant expansion by quantifying its errors and demonstrate its performance on the benchmark problem of N-identical interacting dipoles. We will find exceptional performance even in high-density regimes for different geometries, interesting interpretations of comparisons between correlations and their cumulant expansion, analytically mimic the cumulant expansion procedure and demonstrate its power for the example of an antenna ring.

2 Theory

This section about the underlying theory in this thesis is commenced with a wrap up of two-level systems as well as the inter-atomic coupling via dipole-dipole interaction and followed up by a description of the underlying equations, being the Master and especially the Quantum-Langevin equation. Cumulants and the cumulant expansion will be explained and finally there will be a quick introduction to the very basics of the QuantumCumulants.jl julia package, supported by an example.

2.1 Two-level systems

Almost all systems considered in this thesis are ensembles of equally distributed quantum emitters with two energy levels. The one with higher energy is called the excited state $|e\rangle$ and the one with lower energy ground state $|g\rangle$.
For 2-level systems measurements, rotations, and transformations can be performed via the three well known Pauli matrices and the identity matrix, being

$$\begin{aligned} \sigma_x &= |e\rangle\langle g| + |g\rangle\langle e| \\ \sigma_y &= i(|e\rangle\langle g| - |g\rangle\langle e|) \\ \sigma_z &= |e\rangle\langle e| - |g\rangle\langle g| \\ \mathbb{1} &= |e\rangle\langle e| + |g\rangle\langle g| \end{aligned} \tag{1}$$

They have eigenvalues ± 1 and products of Pauli matrices lead to either unity or another Pauli matrix according to the relation

$$\sigma_\alpha \sigma_\beta = i \sum_\gamma \epsilon_{\alpha\beta\gamma} \sigma_\gamma + \delta_{\alpha\beta} \mathbb{1} \tag{2}$$

Here $\epsilon_{\alpha\beta\gamma}$ denotes the Levi-Civita tensor and $\delta_{\alpha\beta}$ the Kronecker Delta.
From these we can deduce two further, non-Hermitian, operators namely the rising and the lowering operators $\sigma^+ \equiv \sigma^{eg}$ and $\sigma^- \equiv \sigma^{ge}$

$$\begin{aligned} \sigma^+ &= \sigma_x + i\sigma_y = |e\rangle\langle g| \\ \sigma^- &= \sigma_x - i\sigma_y = |g\rangle\langle e| \end{aligned} \tag{3}$$

These operators either transform an emitter in the ground state to the excited state or vice versa.

Another notation used throughout the thesis is the generalized version $\sigma^{ij} = |i\rangle\langle j|$. The sum over all projectors is conserved and equal to unity and from equation 2 a product relation can be deduced

$$\begin{aligned} \sigma^{ij}\sigma^{kl} &= \delta_{jk}\sigma^{il} \\ \sum_{i=1}^{n} \sigma^{ii} &= 1 \end{aligned} \tag{4}$$

where n denotes the total number of possible energy states, being $n = 2$ in the case of the two-level atom. These relations are used to simplify and rewrite equations.

2.2 Dipole-Dipole Interaction

When an atom with transition frequency ω_0 in an ensemble of identical two-level atoms, which can be considered as dipoles, decays from its excited state $|e\rangle$ to the ground state $|g\rangle$, it emits a photon, which can lead to excitation in one of the other ensemble components. This ultimately means the electromagnetic fields of the atoms are coupled to each other - referred to as dipole-dipole interaction - and the surrounding electric vacuum. In order to deduce the corresponding relations, we treat a single quantum emitter in an electromagnetic field, described by the hamiltonian H.

$$H = H_0 + H_{\text{Int}} + H_{\text{F}} \tag{5}$$

$H_0 = \hbar\omega_0\sigma^+\sigma^-$ is the free space hamiltonian for the two-level quantum emitter, where ω_0 is the transition frequency and $\sigma^+ = |e\rangle\langle g|$ is the transition operator shifting the energy level from the ground to the excited state and vice versa σ^- is the adjoint.
$H_{\text{Int}} = -\vec{d}\cdot\vec{E}(0,t)$ is the dipole interaction component of the hamiltonian. By going from the position to the energy basis the interaction term can be rewritten as follows:

$$H_{\text{Int}} = -\vec{d}\cdot\vec{E}(0,t) = \vec{\mu}(\sigma^+ + \sigma^-)\vec{E}(0,t) \tag{6}$$

In order to find an expression for the electric field it can be mode expanded in a box of volume $V = L^3$ with periodic boundary conditions, assuming no external sources and a constant refractive index along the direction of propagation.

$$\vec{E}(\vec{r},t) = \sum_{\vec{k},\lambda} \sqrt{\frac{\hbar\omega_k}{2\epsilon_0 V}} \vec{e}_{\vec{k},\lambda} e^{i\vec{k}\vec{r}} a_{\vec{k},\lambda}(t) \tag{7}$$

This expansion also suggests a splitting of the electric field vector into forward and backward propagating components.

$$\vec{E}(\vec{r},t) = \vec{E}^{+}(\vec{r},t) + \vec{E}^{-}(\vec{r},t) \tag{8}$$

$\vec{e}_{\vec{k},\lambda}$ is the polarization unit vector with $\vec{k}$ being the wave vector and ω_k the frequency corresponding to a field mode and $\lambda \in [1,2]$ the polarization.
$a_{\vec{k},\lambda}$ respectively its adjoint $a^{\dagger}_{\vec{k},\lambda}$ are the bosonic annihilation respectively creation operators, fulfilling the canonical commutation relation $[a_{\vec{k},\lambda}, a^{\dagger}_{\vec{k},\lambda}] = \delta_{\vec{k},\vec{k}'}\delta_{\lambda,\lambda'}$. Using these one can define the hamiltonian for the free electric field:

$$H_{\mathrm{F}} = \sum_{k,\lambda} \hbar\omega_k a^{\dagger}_{\vec{k},\lambda} a_{\vec{k},\lambda} \tag{9}$$

Inserting the mode expanded expression for the electric field into equation 6 gives rise to mixing terms between transition and annihilation/creation operators, although the non-conserving interaction terms can be neglected in the rotating-wave approximation(RWA), namely $\sigma^{+}a^{\dagger}_{\vec{k},\lambda} + \sigma^{-}a_{\vec{k},\lambda}$.
The free-field and interaction hamiltonian can further be trivially generalized to the case of N identical coupled quantum emitters by indexing the position vectors and transition operators to specify on which subsystem they are acting on.
Thus the total hamiltonian from equation 5 takes the following form:

$$\begin{aligned} H = {} & \hbar\omega_0 \sum_j \sigma^{+}_j \sigma^{-}_j + \sum_{\vec{k},\lambda} \hbar\omega_k a^{\dagger}_{\vec{k},\lambda} a_{\vec{k},\lambda} \\ & + \sum_{\vec{k},\lambda} \sum_j \hbar g^{(j)}_{\vec{k},\lambda} \left(\sigma^{+}_j a_{\vec{k},\lambda} e^{i\vec{k}\vec{r}_j} + a^{\dagger}_{\vec{k},\lambda} \sigma^{-}_j e^{-i\vec{k}\vec{r}_j} \right) \end{aligned} \tag{10}$$

$g^{(j)}_{\vec{k},\lambda} = \sqrt{\frac{\omega_k}{2\hbar\epsilon_0 V}} \vec{e}_{\vec{k},\lambda} \vec{\mu}_j$ is the coupling strength of the j-th emitter, but since N identical quantum emitters are treated, the expression simplifies, as $|\vec{\mu}_j| = |\vec{\mu}|$ holds.
Now, in order to capture the time evolution of the annihilation operator, the Heisenberg equation of motion can be utilized, stating:

$$\dot{a}_{\vec{k},\lambda} = \frac{i}{\hbar}[H, a_{\vec{k},\lambda}] = -i\omega_k a_{\vec{k},\lambda} - i \sum_j g_{\vec{k},\lambda} e^{-i\vec{k}\vec{r}_j} \sigma^{-}_j \tag{11}$$

An elegant way to solve this differential equation is to make use of a retarded Green's function corresponding to the present differential operator $L = \partial_t + i\omega_k \rightarrow G(t-t') = e^{-i\omega_k(t-t')}$ and taking boundary conditions into account. The solution is then obtained via convolution of the retarded Green's function with the inhomogeneity:

$$a_{\vec{k},\lambda}(t) = a_{\vec{k},\lambda}(0)e^{-i\omega_k t} - i\sum_j g_{\vec{k},\lambda}e^{-i\vec{k}\vec{r}_j}\int_0^t \sigma_j^-(t')e^{i\omega_k(t'-t)}dt' \tag{12}$$

This gives rise to another splitting of the forward and backward propagating electric field. For the example of the forward propagating field the splitting would be thus

$$\vec{E}^+(\vec{r},t) = \vec{E}^+_{\text{in}}(\vec{r},t) + \vec{E}^+_0(\vec{r},t) \tag{13}$$

with the initial part

$$\vec{E}^+_{\text{in}}(\vec{r},t) = \sum_{\vec{k},\lambda}\sqrt{\frac{\hbar\omega_k}{2\epsilon_0 V}}\vec{e}_{\vec{k},\lambda}e^{i\vec{k}\vec{r}}a_{\vec{k},\lambda}(0)e^{-i\omega_k t} \tag{14}$$

although we assume initial vacuum and thus the term can be neglected. As a side note it would cause quantum noise.
The second term $\vec{E}^+_0(\vec{r},t)$ can be solved using the so-called Markov-Approximation, where one defines an operator $s(t)$ such that

$$\sigma_j^-(t) \propto \sigma_j^-(0)e^{-i\omega_0 t}, \quad s_j^- := \sigma_j^-(t)e^{i\omega_0 t} \propto \sigma_j^-(0) \tag{15}$$

and thus the integral can be simplified as follows

$$\int_0^t dt'\sigma_j^-(t') = s_j^-(t)\int_0^t dt' e^{-i\omega_0 t'} = \sigma_j^-(t)\int_0^t dt' e^{-i\omega_0(t'-t)} \tag{16}$$

which is valid since the time-dependence of the system is encoded primarily in the resonance frequency of the emitters.
Thus the second term in equation 13 reads:

$$E_0^+(\vec{r},t) = -i\sum_{\vec{k},\lambda}\sum_j\sqrt{\frac{\hbar\omega_k}{2\epsilon_0 V}}\vec{e}_{\vec{k},\lambda}g_{\vec{k},\lambda}e^{i\vec{k}(\vec{r}-\vec{r}_j)}\sigma_j^-(t)\int_0^t dt' e^{i(\omega_k-\omega_0)(t'-t)} \tag{17}$$

Utilizing, that polarization unit vectors and wave vectors form an orthonormal basis and going from a sum over the wave vectors to an integral by taking a high density of modes into account, one ends up with a series of integrals, which can be solved and lead to a relation between the transition operators and the electric field, containing the Green's Tensor.

$$\vec{E}^{+}(\vec{r},t) = \vec{E}^{+}_{\text{in}}(\vec{r},t) - \frac{3\hbar\Gamma_0}{4|\vec{\mu}|}\sum_j \sigma_j^{-}(t) G(k_0, \vec{r}-\vec{r}_j)\hat{\vec{\mu}}_j \tag{18}$$

Here $\Gamma_0 = \frac{\omega_0^3|\vec{\mu}|^2}{3\pi c^3 \epsilon_0 \hbar}$ is the single quantum emitter decay rate and

$$G(k,\vec{r}) = e^{ikr}\left[\left(\frac{1}{kr} + \frac{i}{(kr)^2} - \frac{1}{(kr)^3}\right)\mathbb{1} - (\hat{\vec{r}}\circ\hat{\vec{r}})\left(\frac{1}{kr} + \frac{3i}{(kr)^2} - \frac{3}{(kr)^3}\right)\right] \tag{19}$$

is the Green's Tensor for an oscillating dipole. Furthermore $\hat{\vec{r}} = \frac{\vec{r}}{|\vec{r}|}$ is the normalized position vector and $\circ$ denotes the dyadic product.
$\vec{E}^{-}(\vec{r},t)$ can obviously be treated analogously.

It is further possible to define $\xi := kr_{jk}$ and to separate the Greens function into real and imaginary part $G(\xi)$ and $F(\xi)$

$$\begin{aligned} G(\xi) &= -\frac{3}{4}\left[(1-cos^2(\theta))\frac{cos(\xi)}{\xi} - (1-3cos^2(\theta))\left(\frac{sin(\xi)}{\xi^2} + \frac{cos(\xi)}{\xi^3}\right)\right] \\ F(\xi) &= \frac{3}{2}\left[(1-cos^2(\theta))\frac{sin(\xi)}{\xi} - (1-3cos^2(\theta))\left(\frac{cos(\xi)}{\xi^2} - \frac{sin(\xi)}{\xi^3}\right)\right] \end{aligned} \tag{20}$$

to obtain trivial expressions for collective coupling strengths and the collective decay rates.

$$\begin{aligned} \Omega_{jk} &= \Gamma_0 G(k_0, r_{jk}) \\ \Gamma_{jk} &= \Gamma_0 F(k_0, r_{jk}) \end{aligned} \tag{21}$$

The polarization angle θ is measured between the connection line between atoms and the dipole vector $\vec{\mu}$ as shown in the sketch below.
They lead to the intuitive results, that in the so called Dicke limit, when the inter-dipole distance converges to zero, the coupling Ω_{jk} diverges while the collective decay rate converges towards the single emitter decay rate $\Gamma_{jk} \to \Gamma_0$ and for the case of a very large distance $r_{jk} \to \infty$, emitters behave just as single uncoupled quantum emitters, meaning $\Omega_{jk} \to 0$ and $\Gamma_{jk} \to \Gamma_0\delta_{jk}$, as clearly visible in figure 3.

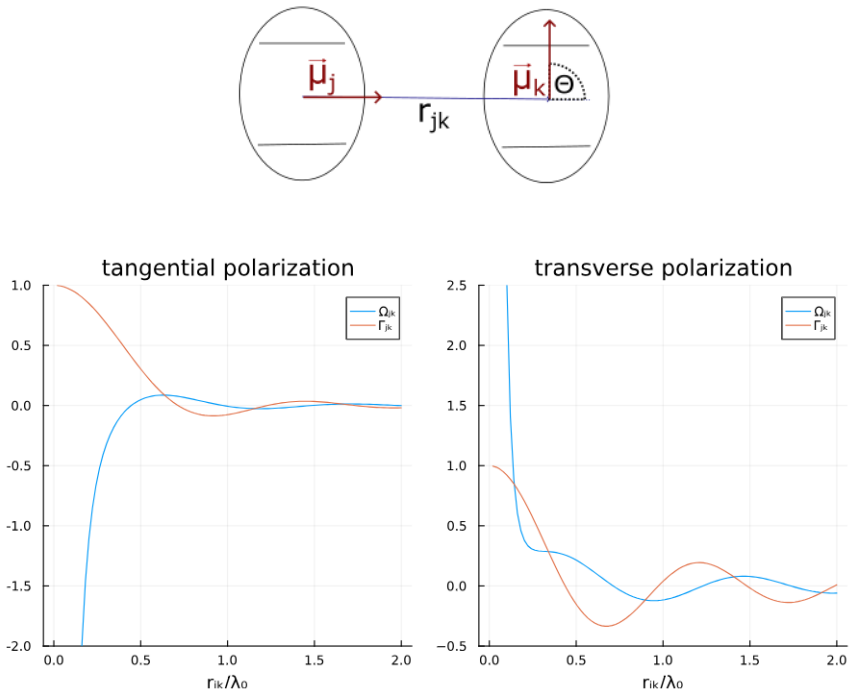

Figure 3: Inter-atomic coupling and collective decay rate from equation 21 dependent on the inter-atomic distance for the case of tangential and transverse polarization. For very small r_{jk} the coupling acts attractively in the tangentially polarized case, i.e. $\Omega_{jk} < 0$, and repulsively in the transversal case vice versa.

2.3 Energy level and decay rate modifications in quantum systems

Spontaneous decay of excited atoms is known to stem from its coupling to vacuum fluctuations of the electro-magnetic field [9]. Further Dicke showed, that coupling of several identical atoms, which lay in the vicinity of each other, leads to correlations and thus to a collective radiation behaviour. In contrast to independent atoms exhibiting a total spontaneous emission intensity proportional to the number of atoms N, collectively decaying atoms, whose radiation changes due to constructive/destructive interference of spontaneously emitted light, display a delayed intensity maximum, which is proportional to N^2[10].

In the case of two two-level atoms there are four collective states in total

$$\{|gg\rangle, |ge\rangle, |eg\rangle, |ee\rangle\} \tag{22}$$

where $|ij\rangle = |i\rangle \otimes |j\rangle$ is a simplified notation and an index indicates which emitter one is referring to. The hamiltonian is given by $H_0 + H_{\text{Int}}$ and thus looks like

$$H = \sum_i \omega_0 \sigma_i^+ \sigma_i^- + \sum_{i,j} \Omega_{ij} \sigma_i^+ \sigma_j^- = \omega_0(\sigma_1^+\sigma_1^- + \sigma_2^+\sigma_2^-) + \Omega(\sigma_1^+\sigma_2^- + \sigma_2^+\sigma_1^-) \tag{23}$$

Diagonalizing the hamiltonian, as done for the coupling and dissipation part in ref. 4, yields the systems Eigenstates, differing from non superposing systems by exhibiting two new states, namely the symmetric $|S\rangle$ and the antisymmetric state $|A\rangle$.

$$\begin{aligned} |G\rangle &= |gg\rangle \\ |S\rangle &= \frac{1}{\sqrt{2}}(|eg\rangle + |ge\rangle) \\ |A\rangle &= \frac{1}{\sqrt{2}}(|eg\rangle - |ge\rangle) \\ |E\rangle &= |ee\rangle \end{aligned} \tag{24}$$

The new states have corresponding coupling induced modified energies $E_{S/A} = \omega_0 \pm \Omega$ and thus the degeneracy is lifted, while $|E\rangle$ and $|G\rangle$ remain at their respective energies. The states $|S\rangle$ and $|A\rangle$ are also part of the Bell basis. For very small inter-subsystem spacings r, the coupling diverges and would lead to $\pm\infty$ energy. This distance, where the model breaks down, is about the Bohr radius.

The through coupling modified energy level scheme exhibits two independent decay channels $\gamma_{S/A} = \Gamma_0 \pm \gamma$ depending on wether the collective excited state decays via the symmetric or the antisymmetric state. γ is given by $\gamma = \Gamma_0 F(k_0, r)$ and for $\gamma > 0$ the channel including the symmetric state shows a higher decay rate than the single atom decay rate Γ_0 and is thus called "superradiant". The opposite case of a reduced decay rate for the channel including the antisymmetric state is therefore called subradiant.

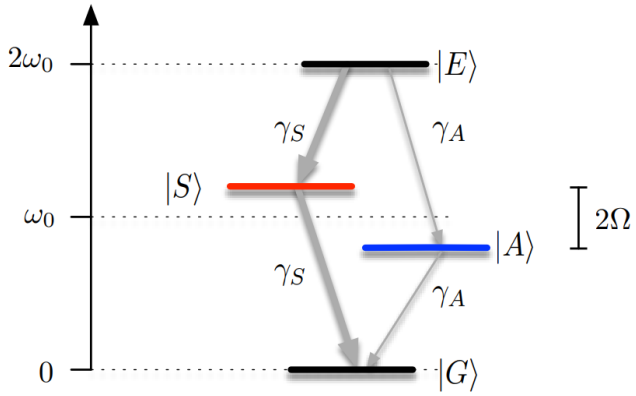

Figure 4: Visualization of the modification of the energy levels in a two atom system, shifted by $\pm\Omega$ for the super- respectively subradiant state accompanied by two non-interacting decay channels γ_S and γ_A when involving the symmetric or the antisymmetric state[9]

.

2.4 Fundamental equations in quantum physics

2.4.1 Master equation

In order to find the time evolution of the state defining density matrix under consideration of dissipative effects one has to solve the Master Equation. Here we derive it for the problem of N identical coupled quantum emitters to which end an expression for the electric field was derived in section 2.2.

The time evolution of a density matrix $\rho = \sum_j p_j |\Psi_j\rangle\langle\Psi_j|$, where p_j are the weights associated with different quantum states $|\Psi_j\rangle$ and which satisfy the condition $\sum_j p_j = 1$ to ensure that the total probability adds up to one, is computed using the well known von Neumann equation with the time evolution determining hamiltonian from equation 5.

$$\begin{aligned}\dot{\rho} &= -\frac{i}{\hbar}[H,\rho] = -\frac{i}{\hbar}[H_0 + H_{\text{Int}},\rho] \\ &= -\frac{i}{\hbar}[H_0,\rho] - \frac{i}{\hbar}\sum_j \left[[\sigma_j^+,\rho](\vec{\mu}_j \cdot \vec{E}^+(\vec{r}_j)) + (\vec{\mu}_j \cdot \vec{E}^-(\vec{r}_j))[\sigma_j^-,\rho]\right]\end{aligned} \tag{25}$$

Now the expression for the electric field[17] can be inserted, exemplary shown for the electric field in forward direction term.

$$\begin{aligned}&-\frac{i}{\hbar}\sum_j [\sigma_j^+,\rho](\vec{\mu}_j \cdot \vec{E}^+(\vec{r}_j)) = \\ &-\frac{i}{\hbar}\sum_k [\sigma_k^+,\rho]\left(\vec{\mu}_k \cdot \vec{E}_{in}^+(\vec{r}_k) - \frac{3\hbar\Gamma_0}{4}\sum_j \sigma_j^-(t)\hat{\vec{\mu}}_k \cdot G(k_0,\vec{r}_k - \vec{r}_j)\cdot\hat{\vec{\mu}}_j\right)\end{aligned} \tag{26}$$

Doing the analogue for the backward propagating electric field, splitting the Green's Tensor into real and imaginary part aswell as redefining $\vec{r}_{kj} = \vec{r}_k - \vec{r}_j$ for simplicity leads to the following equation:

$$\begin{aligned}\dot{\rho} = &-\frac{i}{\hbar}[H_0, \rho] + \frac{3i\Gamma_0}{4}\sum_{k,j}[\sigma_k^+\sigma_j^-, \rho]\left(\hat{\vec{\mu}}_k \cdot \Re(G(K_0, \vec{r}_{kj})) \cdot \hat{\vec{\mu}}_j\right) \\ &- \sum_k [\sigma_k^+, \rho]\left[\frac{i}{\hbar}\vec{\mu}_k \cdot \vec{E}_{in}^+(\vec{r}_k) + \frac{3\Gamma_0}{4}\sum_j\left(\hat{\vec{\mu}}_k \cdot \Im(G(k_0, \vec{r}_{kj})) \cdot \hat{\vec{\mu}}_j\right)\sigma_j^-\right] \\ &- \sum_k \left[\frac{i}{\hbar}\vec{\mu}_k \cdot \vec{E}_{in}^-(\vec{r}_k) - \frac{3\Gamma_0}{4}\sum_j\left(\hat{\vec{\mu}}_k \cdot \Im(G(k_0, \vec{r}_{kj})) \cdot \hat{\vec{\mu}}_j\right)\sigma_j^+\right][\sigma_k^-, \rho]\end{aligned} \tag{27}$$

To break this large equation further down, the quantum noise operators can be defined for the quantum noise generating term in the electric fields $\vec{E}_{\text{in}}^{\pm}$ as well as their arising commutation relation.

$$\begin{aligned}\xi_j^-(t) &:= \frac{i}{\hbar\sqrt{\Gamma_0}}(\vec{\mu}_j\vec{E}_{in}^+(\vec{r}_j, t)) = \frac{i}{\sqrt{\Gamma_0}}\sum_{\vec{k},\lambda} g_{\vec{k},\lambda}a_{\vec{k},\lambda}(0)e^{-i\omega_k t}e^{i\vec{k}\vec{r}_j} \\ [\xi_m(t), \xi_n^\dagger(t')] &= \frac{3}{2}\delta(t-t')\hat{\vec{\mu}}_m \cdot \Im(G(k_0, \vec{r}_{mn})) \cdot \hat{\vec{\mu}}_n\end{aligned} \tag{28}$$

The expression for the Master Equation for N coupled identical quantum emitters thus becomes

$$\begin{aligned}\dot{\rho} = &-\frac{i}{\hbar}[H_0 + H_{\text{dip}}, \rho] - \sum_{j,k}[\sigma_j^+, \rho](\delta_{jk}\sqrt{\Gamma_0}\xi_j^-(t) + \frac{\Gamma_{jk}}{2}\sigma_k^-) \\ &+ \sum_{j,k}(\delta_{jk}\sqrt{\Gamma_0}\xi_j^+(t) + \frac{\Gamma_{jk}}{2}\sigma_k^+)[\sigma_j^-, \rho]\end{aligned} \tag{29}$$

with a more treatable formulation of the dipole interaction hamiltonian.

$$H_{\text{dip}} = \sum_{j,k}\hbar\Omega_{jk}\sigma_j^+\sigma_k^- \tag{30}$$

where Ω_{jk} is the coupling strength between dipole j and k and Γ_{jk} the collective decay rate.

$$\begin{aligned}\Omega_{jk} &= -\frac{3\Gamma_0}{4}\hat{\vec{\mu}}_j \cdot \Re(G(k_0, \vec{r}_{jk})) \cdot \hat{\vec{\mu}}_k \\ \Gamma_{jk} &= \frac{3\Gamma_0}{2}\hat{\vec{\mu}}_j \cdot \Im(G(k_0, \vec{r}_{jk})) \cdot \hat{\vec{\mu}}_k\end{aligned} \tag{31}$$

2.4.2 Quantum Langevin equation

An equivalent way to calculate the time evolution of a system is to use the Quantum Langevin equation. Going from the Master to the Quantum Langevin equation is equivalent to going from the Schroedinger to the Heisenberg picture and shifting the time dependence from the state vector to the operators. When using the unitary time evolution operator $U(t) = e^{-\frac{i}{\hbar}Ht}$ with its action on a state vector $U(t)|\Psi(0)\rangle = |\Psi(t)\rangle$ and the transformation of an operator from the Schroedinger picture O_S to the Heisenberg picture O_H given by $U(t)O_\mathrm{S}U^\dagger(t) = O_\mathrm{H}$, we can derive an expression for the time derivative of the expectation value of operator O.

$$\langle \dot{O} \rangle = Tr(\dot{\rho} \cdot O) \tag{32}$$

Using this and tracing over the whole Master equation [29] while making use of the cyclic property of the trace $Tr(ABC) = Tr(BCA) = Tr(CAB)$, one can find an expression for the time evolution of operator O.

$$\begin{aligned} \dot{O} =& \frac{i}{\hbar}[H, O] + \sum_{jk} [\sigma_j^+, O] \left(\delta_{jk} \sqrt{\Gamma_0} \xi_j^-(t) + \frac{\Gamma_{jk}}{2} \sigma_k^- \right) \\ & - \sum_{jk} \left(\delta_{jk} \sqrt{\Gamma_0} \xi_j^+(t) + \frac{\Gamma_{jk}}{2} \sigma_k^+ \right) [\sigma_j^-, O] \end{aligned} \tag{33}$$

This is the Quantum Langevin equation for operators O, which commute at equal times with the bosonic ladder operators a and $a^\dagger$.

The Quantum Langevin equation provides the same information as the master equation. But since we are mostly interested in averages, we can simplify the Quantum Langevin equation by assuming any occurring noise to be white noise so averages over the quantum noise operators ξ_j vanish, and use the following equation for computation.

$$\dot{O} = \frac{i}{\hbar}[H, O] + \sum_{j,k} \Gamma_{jk} (\sigma_k^+ O \sigma_j^- - \frac{1}{2} \{\sigma_j^+ \sigma_k^-, O\}) \tag{34}$$

It is trivial to proof, that both approaches, using the Quantum Langevin and the master equation, generate the same results e.g. for the time evolution of expectation values, which is equivalent to the comparison between the solutions for expectation values calculated via the density matrix ρ, gained from the master equation, and the solutions obtained by applying an averaging to the operator O given by a corresponding Quantum-Langevin equation.
So we need to show, that

$$\langle O \rangle = Tr(\rho(t) \cdot O) = Tr(\rho \cdot O(t)) \tag{35}$$

which is simple, when considering the time evolution operator $U(t)$ stemming from the Schroedinger equation. With $\rho = U(t)\rho U^{\dagger}(t)$, the hermitian property of $U(t)$ and the cyclic property of the trace we can move the time dependence from the density matrix to the operator.

$$Tr(\rho(t) \cdot O) = Tr(U(t)\rho U^{\dagger}(t)O) = Tr(\rho U^{\dagger}(t)OU(t)) = Tr(\rho O(t)) \tag{36}$$

Hence averages over operator entries reproduce the exact solution and all correlations between the atoms are covered.

2.5 Cumulant expansion

When solving the Quantum Langevin or the master equation, the entire information about the system is obtained, although maybe only some specific expectation values are needed for computation. Inserting any operator into the Quantum Langevin equation leads to a complex operator equation, but averaging over these transforms them into more tractable c-number equations. But calculating equations of motion for an exemplary model like e.g. the Jaynes-Cummings model, done in ref. 5, quickly visualizes, that this does not break down the complexity either, as the equations contain averages of ever longer operator products, whose equations of motion have to be calculated as well, not leading to a closed set of equations.
Thus in order to find a solution some sort of approximation is necessary.
One adequate approximation is the cumulant expansion, initially introduced by R. Kubo [7], which is based on the expansion of averages of higher-order operator products in terms of lower order expectation values.

In probability theory one obtains moments for a set of statistical variables $\boldsymbol{X} = \{X_1, X_2, ..., X_n\}$ via a moment generating functional $M_{\mathrm{X}}[j]$

$$M_{\mathrm{X}}[j] = \langle e^{j\mathrm{X}} \rangle \tag{37}$$

for a parameter vector $j \in \mathbb{R}^n$ and n being the dimension of vector $\boldsymbol{X}$.
By taking the natural logarithm of $M_{\mathrm{X}}[j]$ we obtain the corresponding cumulant functional $K_{\mathrm{X}}[j]$, which can be expressed as power series containing the n-th cumulant κ_n, which then can be obtained by taking the n-th derivative at $j = 0$ by construction.

$$\begin{aligned} K_{\mathrm{X}}[j] &= \sum_{n=1}^{\infty} \frac{j^n}{n!} \kappa_n \\ \kappa_n &= \frac{\mathrm{d}^n}{\mathrm{dj}^n}\Big|_{j=0} K_{\mathrm{X}}[j] \end{aligned} \tag{38}$$

The first four cumulants (sometimes called semi-invariants) are often referred to as mean, variance, skewness and kurtosis.

An example would be the cumulants of a normal distribution $\mathcal{N}(\mu, \sigma)$ of a random variable X, for which the cumulant generating function can be found to be

$$\begin{aligned} K_{\mathrm{X}}[j] &= ln\langle e^{j\mathrm{X}}\rangle = ln(\int \mathrm{dX} e^{j\mathrm{X}} \mathcal{N}(\mu,\sigma)) \\ &= ln(\int \mathrm{dX} e^{j\mathrm{X}} \frac{1}{\sqrt{2\pi}\sigma} e^{-\frac{1}{2}(\frac{\mathrm{X}-\mu}{\sigma})^2}) \\ &= ln(\int e^{j(z\sigma+\mu)} \frac{1}{\sqrt{2\pi}\sigma} e^{-\frac{1}{2}z^2} |\frac{\mathrm{dX}}{\mathrm{d}z}| \mathrm{d}z) \\ &= ln(e^{\mu j} \int e^{jz\sigma} \frac{1}{\sqrt{2\pi}} e^{-\frac{1}{2}z^2} \mathrm{d}z) \\ &= ln(e^{\mu j + \frac{1}{2}\sigma^2 j^2}) = \mu j + \frac{1}{2}\sigma^2 j^2 \end{aligned} \tag{39}$$

In the third step $\mathrm{X} = z\sigma + \mu$ was substituted, so that $\left|\frac{\mathrm{dX}}{\mathrm{d}z}\right| = \sigma$ and in the fourth we used, that $\int e^{zj} \frac{1}{\sqrt{2\pi}} e^{-\frac{1}{2}z^2} \mathrm{d}z = e^{\frac{j^2}{2}}$.

Therefore the cumulants are indeed the mean, the variance and all cumulants of order ≥ 3 vanish for this specific probability distribution with a centered gaussian.

$$\begin{aligned} \kappa_1 &= \mu \\ \kappa_2 &= \sigma^2 \\ \kappa_n &= 0 \quad \forall \quad n \geq 3 \end{aligned} \tag{40}$$

In general odd cumulants, being related to skewness, provide information about the direction and extent of the asymmetry in a probability distribution and are thus particularly useful when describing asymmetric systems and vice versa even cumulants for symmetric systems.

On this whole basis a joint cumulant as a measure for the correlations between statistical variables can be alternatively defined for a product of order n of a set of statistical variables $\boldsymbol{X}$ and is denoted by $\langle \cdot \rangle_C$

$$\langle X_1 X_2 ... X_n \rangle_C = \sum_{p \in P(I)} (|p|-1)!(-1)^{|p|-1} \prod_{B \in p} \langle \prod_{i \in B} X_i \rangle \tag{41}$$

where $I = 1, ..., n$, $P(I)$ is the set of all partitions of I, with the number of partitions being given by the Bell numbers, $|p|$ the length of the partition p and B runs over the blocks of each partition.

To clarify the process, it is shown for the example $n = 3$ with the following joint cumulant

$$\begin{aligned}\langle X_1X_2X_3\rangle_C =&\langle X_1X_2X_3\rangle - \langle X_1X_2\rangle\langle X_3\rangle - \langle X_1X_3\rangle\langle X_2\rangle \\ &- \langle X_1\rangle\langle X_2X_3\rangle + 2\langle X_1\rangle\langle X_2\rangle\langle X_3\rangle\end{aligned} \tag{42}$$

R. Kubo proposed that the statistical variables may be quantum operators instead and the cumulant expansion method follows from Theorem I in ref. 7, which states that the joint cumulant of a set of operators is zero if any one (or any subset) of them is statistically independent of the others. So if simply assuming, that the joint cumulant of a given order is zero, we obtain an expression of an average in terms of only lower-order averages. Equation 42 thus becomes

$$\langle X_1...X_n\rangle = \sum_{p\in P(I)\backslash I} (|p|-1)!(-1)^{|p|} \prod_{B\in p} \langle \prod_{i\in B} X_i\rangle \tag{43}$$

with $P(I)\backslash I$ as the set of all partitions of I not containing I itself. For the example of $n = 3$ we end up with the following equation

$$\begin{aligned}\langle X_1X_2X_3\rangle =&\langle X_1X_2\rangle\langle X_3\rangle + \langle X_1X_3\rangle\langle X_2\rangle \\ &+ \langle X_1\rangle\langle X_2X_3\rangle - 2\langle X_1\rangle\langle X_2\rangle\langle X_3\rangle\end{aligned} \tag{44}$$

The cumulant expansion can be used recursively until arriving at first order, which corresponds to the lowest order mean-field approximation and renders the dynamics of the system under consideration classical.

The cumulant expansion can greatly reduce the problem complexity by breaking down the amount of equations of motion to something numerically or for small problems even analytically solvable.

2.6 Introduction to the QuantumCumulants.jl package

QuantumCumulants.jl is a package inside the julia programming language and capable of performing the cumulant expansion up to any desired order. It is easy to use and supported by a detailed documentation [8].
One commences by defining c-numbers as symbolic variables, as well as the hilbert space and the occuring operators.

```
using QuantumCumulants
@cnumbers ω η
Γ(i,j) = cnumbers(Symbol(Γ, i, j))[1]
Ω(i,j) = cnumbers(Symbol(Ω, i, j))[1]

ha = ⊗([NLevelSpace(Symbol(:atom,i),2) for i=1:N]...) #hilbert space
σ(i,j,k) = Transition(ha, Symbol("σ_{$k}"),i,j,k)
```

Next one defines hamiltonian, jump operators and decay rates and specifies the operators of interest.

```
H = sum(Ω(i,j)*σ(2,1,i)*σ(1,2,j)*(i≠j) for i=1:N for j=1:N) #hamiltonian

J = [σ(1,2,k) for k=1:N] #jump operator for eqs()
rates = [Γ(i,j) for i=1:N, j=1:N] #decay rates
ops = [σ(2,2,i) for i=1:N]
```

Now we can use the meanfield() function to generate the equation of motion according to the modified Quantum Langevin equation [53] for the operators of interest and cumulant expand it up to a specified order. Then the complete!() function scans for right-hand-side terms in the e.o.m., which are not appearing on the left and calculates the cumulant expanded e.o.m. for these as well, yielding the complete system of coupled differential equations.

```
order = 2
eqs = meanfield(ops, H, J; rates=rates, order=order)
complete!(eqs)
```

One can then transform the completed equations to an ordinary differential equation system object, pass a set of parameters for the former defined symbolic variables and numerically solve this. The package also offers functions to calculate the correlation function between two operators, their spectrum and much more. For more information please refer to the corresponding documentation in ref. [8].

3 Validity of the cumulant expansion approximation

Currently quantum simulations of systems of large size are rarely feasible without approximation methods and thus the cumulant expansion plays an important role in getting insight into the dynamics of large complex systems.
But this is only valid of course under the condition, that the approximation performs sufficiently well.
An estimation of its performance under a variety of conditions is crucial to figure out for which cases this approach is even viable or if it is viable at all.
Therefore different systems will be simulated under variation of parameters, which either change its time evolution or the system itself. The analyzed relevant parameters are the interatomic distance d, the polarization angle θ, being measured relative to the connection line of the atoms, the system size and the geometry. But also the impact of choosing a certain initial state and the effect of a driving term in the hamiltonian will be discussed where it is causing relevant discrepancy.

3.1 Chain and ring geometry

First let us specify the geometries of the quantum arrays we use.
We will focus on chains and rings of N identical point-like quantum emitters.
In the case of the chain one simply transforms $\xi \to \xi \cdot |j - i|$ in equations 21 and sums over the atom indices i and j to calculate the total coupling and decay rates between every atom and for every decay channel in an all-to-all connected scenario. The dipole vector orientation will be controlled by the angle θ measured between dipole orientation and the connection line between the atoms.
In the case of the ring we have to pass position and dipole moment vectors to Ω and Γ.

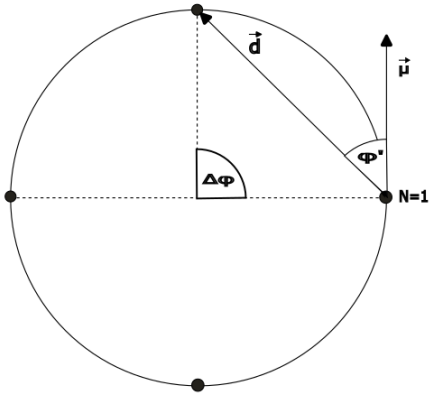

Figure 8: Sketch of an arbitrary ring with $N = 4$ for visualizing purposes.

First the angle for the position of an atom $j \in \{1, 2, ..., N\}$ is $\phi(j) = \frac{2\pi(j-1)}{N}$, measured in the x-y-plane. The angle ϕ' between connection vector $\vec{d}$ and polarization vector $\vec{\mu}$ is trivially given by $\phi' = \frac{\phi}{2}$, defined for $\phi' \in [0, \pi]$.
Second follows from geometrical considerations, that

$$\frac{d}{2} \cdot \frac{1}{R} = sin(\frac{\Delta\phi}{2}) \iff R(d) = \frac{d}{2sin(\frac{\Delta\phi}{2})} = \frac{d}{2sin(\frac{\pi}{N})} \tag{45}$$

for the radius, using the angle $\Delta\phi$ between the radial vectors of two neighbouring dipoles, given by $\Delta\phi = \frac{2\pi}{N}$ for equal distribution. Now, by going over the atom index j and specifying the inter atomic distance d, we fully specify the position vector.

3.2 Hamiltonian and simulation details

Averages over operator entries obtained from the Quantum Langevin equation are exact. However similar computational effort is necessary compared to the master approach and therefore one only gains time when using lower order correlations by e.g. performing the cumulant expansion.
We will proceed by estimating the performance of the cumulant expansion in the following sections, but need to specify the hamiltonian as part of the corresponding Quantum Langevin equation beforehand.
In our case the basic hamiltonian for our system of identical point-like two-level quantum emitters is the sum of the free-field atom hamiltonian H_0 and the dipole hamiltonian H_{dip}:

$$\begin{aligned} H_0 &= \sum_{j}^{N} \omega \sigma_j^+ \sigma_j^- \\ H_{\text{dip}} &= \sum_{i}^{N} \sum_{j}^{N} \Omega_{ij} \sigma_i^+ \sigma_j^- \quad \forall\ i \neq j \end{aligned} \tag{46}$$

Here ω is the transition frequency between the two energy levels of our two-level atoms, Ω_{ij} is the coupling between atom i and j. σ_i^+, σ_i^- are the jump operators acting on atom i described in equation 3.
We neglect terms with $i = j$, because we consider ensembles of identical atoms and the self-coupling thus induces an identical energy shift in every atom. Therefore the self-coupling is irrelevant for studying dynamics.

However if the system is desired to be initially in the collective ground state, this hamiltonian does never lead out of it, although it is advantageous to have this initial state, as there is no automated way for correctly defining different initial states in the QuantumCumulants.jl package yet and for large systems it can get quite time consuming finding them manually. Besides that starting in the initial ground state is unavoidable for most experimental realizations. Therefore in order to force a dynamic it is necessary to add a so called driving term, which can have a variety of shapes. For the following simulations it will be mostly chosen as a simultaneous pumping of all atoms up to a certain time. We will also drop the phase terms in our driving hamiltonian H_{drive}, as we will work with perpendicular radiation of our two-dimensional arrays and thus H_{drive} is given via equation 47

$$H_{\text{drive}} = \sum_{i}^{N} \eta(\sigma_i^+ + \sigma_i^-) \cdot P(t) \tag{47}$$

and the hamiltonian for most of the upcoming simulations - unless stated differently - is thus

$$H = H_0 + H_{\text{dip}} + H_{\text{drive}}. \tag{48}$$

As a side note one could realize such a driving for example via an external laser. η defines the pumping strength, which is set to $\eta = \Gamma_0$ in the upcoming simulations and $P(t)$ will be a step-function, although it can be chosen arbitrarily.

$$P(t) = \begin{cases} 1 & \Gamma_0 \cdot t < 5, \\ 0 & \Gamma_0 \cdot t \geq 5 \end{cases} \tag{49}$$

This choice ensures, that both driven and non-driven dynamics are captured.
The upper state population or the probability to find an atom in the excited state, being described by the expectation value of the transition operator $|e\rangle\langle e|_i$ or σ_i^{ee} for an atom i, which projects the time average of the transition from the excited state to itself, is the mainly considered operator in this thesis.
Since the task is to capture the dynamics of the system and to evaluate the performance of the cumulant expansion, it is sufficient to work with natural units in the simulations, i.e. $\hbar = 1$.

3.3 Error measure

To find possible systematics in performance decrease or increase when performing a cumulant expansion, we need to define an error measure for the difference between exact and approximated solution.

In this section we quantify the difference between operator expectation value dynamics in different orders of cumulant expansion and in order to do so, we need to define an error measure.

Although there is in general a variety of such, it is desirable to choose a measure which is cumulative, so it covers all occuring deviations, and is using absolute values, so positive and negative differences do not cancel out. One measure fitting these requirements in a simple and intuitive manner is a modified version of the so called "City-Block distance" or "Manhattan distance" [11] divided by the length of the time vector n. We will refer to it as "normalized City-Block error" (NCBE)

$$\text{NCBE} = \frac{1}{n} \sum_{i}^{n} |\hat{y}_i - y_i| \tag{50}$$

with $\hat{y}_i$ and y_i being the function value at time bin i of the actual respectively the predicted values. The NCBE is symmetric with respect to its arguments. This error is used instead of more standard error measures like for example the equivalent standard deviation for visualizing reasons, as the standard deviation happens to be extremely small for the occuring differences. In the context of this thesis the actual values will mostly correspond to the values of the exact solution and the predicted ones to the lower order solution values.

3.4 Validity dependent on polarization and inter-atomic distance

The time evolution of transition operators in our considered quantum optical systems depends amongst other parameters on the coupling strength between the dipoles $\Omega_{ij}(d, \theta)$ as well as the collective decay rates $\Gamma_{ij}(d, \theta)$ which in turn depend on the atomic spacing d and their polarization θ. We will quantify how different orders perform relative to the exact solution, starting with the difference between exact and mean field solution for a system of two atoms starting in the collective excited state without external driving when varying spacing d and polarization θ, where $\theta = 0$ is longitudinal and $\theta = \frac{\pi}{2}$ transversal polarization.

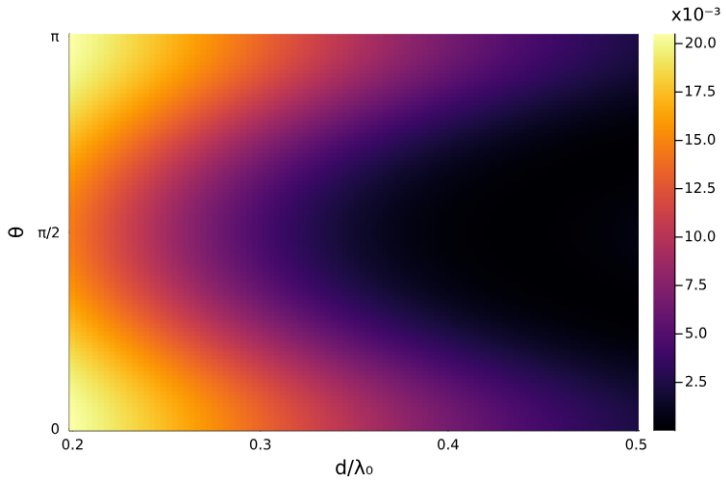

Figure 9: NCBE for a non driven system initially in the collective excited state of two atoms for simulations over a time span of $\Gamma_0 \cdot t \in [0, 10]$ while varying inter-atomic spacing d and polarization θ. The excited state population expectation value $\langle \sigma^{22} \rangle$ is compared in 2nd and 1st order. It will be in theory averaged over all atoms, but due to the symmetry $\langle \sigma_1^{22} \rangle = \langle \sigma_2^{22} \rangle$ holds in this particular case so we only have to compute the excited state population of a single atom.

The deviations are not surprising at all. While in first order atoms are independent and decay exponentially with Γ_0, their coupling modifies their decay rate when considering correlations between the atoms. It is observed, that the first order cumulant expansion or classical solution differs more from the exact solution or in other words "gets worse" the stronger the coupling and collective decay rate is, i.e. the smaller d gets or the larger the density. On another note the NCBE behaves like a superposition of π-periodic trigonometric functions, stemming from the trigonometric polarization dependence in the coupling and collective decay rate functions [21].

Apart of that we find improved approximation results for transverse polarization compared to tangential polarization with more tolerance to the same error for about $d \approx 0.12\lambda_0$, since the electric field in the former case couples weaker to the other dipole.
However the results change drastically when going back to a driven system.

3.5 Ω and Γ zero-crossings

Before doing so, we will explain the shape of figure 9 by plotting the collective coupling constant $\Omega_{ij}(d,\theta)$ and the collective decay rate $\Gamma_{ij}(d,\theta)$. We will see that the error map is in full agreement with the coupling map and that there would technically be one more dip related to the collective decay rate too small to resolve.
The underlying idea is, that since higher order correlations in our equations of motion stem from operator products arising from either the interaction hamiltonian or the dissipative term in the corresponding Quantum-Langevin equation, they are all weighted by either a coupling $\Omega_{ij}(d,\theta)$ or a decay rate $\Gamma_{ij}(d,\theta)$. If in an extreme case all of these quantities vanish simultaneously, only lower order correlations remain in our equations of motion, leading to full agreement between the exact and the first order cumulant expanded solution. These quantities however do not generally vanish simultaneously, so there will only be improvement but no exact solution obtained, when cumulant expanding the equations of motion.
Hence it plays an important role in the estimation of the cumulant expansion performance, we quantify where the coupling and decay rates defined in equation 21 are almost or equal to zero for a system of two and a system of three atoms and we will refer to it as "zero-crossings".
In driven systems error peaks will occur far beyond the first zero-crossing, leading to irrelevance of this error influential parameter, while in the non-driven case in figure 9 it basically solely defines the error map. There we compare results in different orders and the error map follows exactly $\Gamma_{12}(d,\theta)$.
When going to larger systems, additional decay channels and couplings to next neighbours arise, leading logically to more zero-crossings of higher order correlation terms due to the zero-crossings of the parameters in smaller and smaller regimes as well. One can imagine, that such a map like figure 12 will be almost completely dark for systems of length 5 already. This further motivates the cumulant expansion for larger systems, as the error reducing action of this effect increases with the number of coupling and dissipation terms.

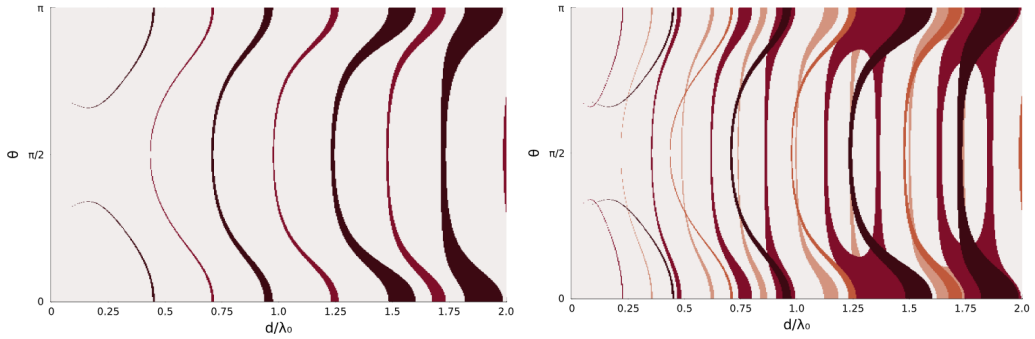

Figure 12: A heatmap showing all spots of the coupling and collective decay functions, where they are close to zero, hinting, but not solely determining, parameter vectors, where a cumulant expansion approach is valid. On the left are the zero-crossings for a system of two dipoles and on the right for three dipoles, having additional zero-crossings for the coupling between first and third atom and for the additional decay channel as well. Black: Ω_{12}, Brown: Ω_{13}, Orange: Γ_{12}, Skin color: Γ_{13}. Dips arising from weaker components, like e.g. Γ_{13}, will contribute less to a cumulant expansion performance increase than e.g. Ω_{12}.

Since the inter subsystem spacing d occurs inside of Ω_{ij} and Γ_{ij} as argument in trigonometric functions and denominators, increasing system size while keeping density constant leads to weaker contributions of associated coupling and decay rate as well as faster oscillations and thus more frequent zero-crossings, simply due to the form of the functions.

3.6 Driven systems

When applying an external drive to a system with sub wavelength spaced atoms initially in the collective ground state, the NCBE of operator dynamics in different orders, primarily controlled by the hamiltonian, is determined by the counteraction between higher order and lower order inducing terms, i.e. coupling and dissipation versus driving and free-field atom term in our case. While the interaction term introduces higher order correlations, the chosen driving term, resembling a laser drive, does not and thus a dominating driving term results in improved lower order results and a dominating coupling term vice versa.
In figure 13 it is shown how the interaction between atoms only gets relevant at a certain amount of dynamics happening. Something similar to power broadening appears, where only enough power is necessary to force dynamics and hence observe these. Consequently significant errors are only induced by interaction when pumping with sufficient strength.

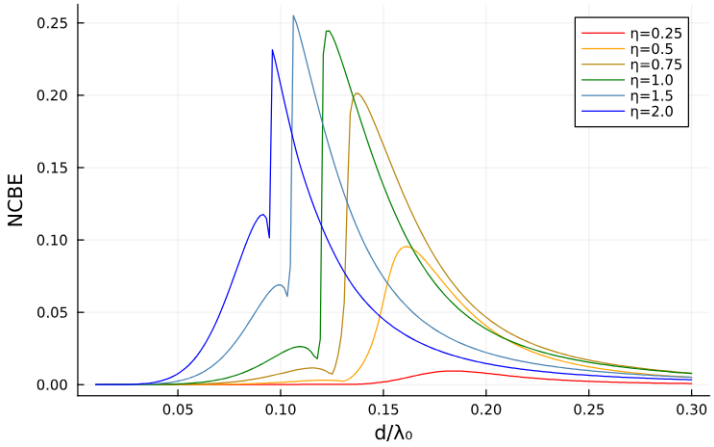

Figure 13: NCBE for the collective excited state population in 2nd and 1st order dependent on d for different pumping strengths η, when pumping constantly over the whole simulation duration. Subsystems are tangentially polarized and simulated for time spans $\Gamma_0 \cdot t \in [0, 10]$. Clearly the peaks shift to the left when increasing pumping strength.

Also stronger pumping obviously requires stronger coupling, i.e. smaller inter-atomic spacing, to be dominated and thus the peaks shift towards smaller spacing with stronger pumping.
Having strong coupling $\Omega >> \eta$ locks the system in the ground state again, making changes to it require even stronger pumping and therefore a mean-field approach is feasible again, but only since no or little dynamics will be observable at all.

This ultimately means, that the comparison between different order cumulant expansion results can be utilized to sense for parameter regimes maintaining a balance between well observable dynamics and the occurrence of quantum effects.

The same effect as terms with η arising from the driving hamiltonian H_{drive} have terms with ω stemming from the other lower order inducing term H_0. Even in the case of a closed system the time evolution of the excited state population of atom m $\dot{\sigma}_m^{22}$ is dependent on ω despite the commutator $[H_0, \sigma_m^{22}]$ vanishing, since σ^{22} commutes with itself, because it depends on the ladder operators via the driving term and these are in turn dependent on ω and therefore $\dot{\sigma}_m^{22}$ does.

This can be trivially shown by solving the Heisenberg-equation using the terms of interest for one jump operator and the other will be given by the complex conjugate.

$$\begin{aligned}
\dot{\sigma}_m^{21} &= \frac{i}{\hbar}[H_0 + H_{\text{drive}}, \sigma_m^{21}] \\
&= \frac{i}{\hbar}[\sum_j (\omega\sigma_j^{22} + \eta(\sigma_j^{21} + \sigma_j^{12})), \sigma_m^{21}] \\
&= \frac{i}{\hbar}(\omega\sigma_j^{21}\delta_{jm} + [\sum_j \eta\sigma_j^{12}, \sigma_m^{21}]) \\
&= \frac{i}{\hbar}\delta_{jm}(\omega\sigma_j^{21} + \eta(\sigma_j^{11} - \sigma_j^{22})) \\
&= \frac{i}{\hbar}\delta_{jm}(\omega\sigma_j^{21} - \eta\sigma_j^{z})
\end{aligned} \tag{51}$$

This consequently means $\sigma_m^{22} \equiv \sigma_m^{22}(\omega)$ and again larger values of ω result in a shift of the peak to the left, i.e. towards stronger coupling.
In the case of $\dot{\sigma}_m^{21}$ for two atoms ω would have a slightly lower impact on the peak shift than η simply because the expectation value it weights is smaller.

3.6.1 Error peaks in higher orders

The effect causing the peaks in figure 13 not only occurs for the comparison to the solution under classical consideration, i.e. the cumulant expansion up to first order, but for comparisons of arbitrary orders for arbitrary geometries, as this effect is based on general correlations, as shown in figure 14 for a dipole chain of length 3.
We can also observe special behaviour at polarizations $\theta_m \approx \pm 54.7° + n \cdot 180°$ with $n \in \mathbb{Z}$ for the first time, being the magic angles. At these specific angles $\Omega_{ij}(d, \theta)$ is zero thus resulting in a smaller NCBE compared to other polarizations.
As a side note the magic angle does not occur for the non-driven case in figure 9 due to the initial conditions. The excited state population dynamic exhibits no oscillations, which are connected to the energy shift Ω_{12}, and only decays described by a sum of exponentials containing Γ_0 and Γ_{12}. Consequently it is not affected by the magic angle. Hints for this behaviour will be given in section 4.1.

The peak appears for the comparison of every order at the same parameters, only the errors amplitude and the specific peak shape changes when varying the orders one considers or, as we will see later on, when varying pump type or pump strength. Logically the error is higher for higher order differences, as going down in orders means neglecting more and more correlations, hence increasingly deviating from the exact solution.

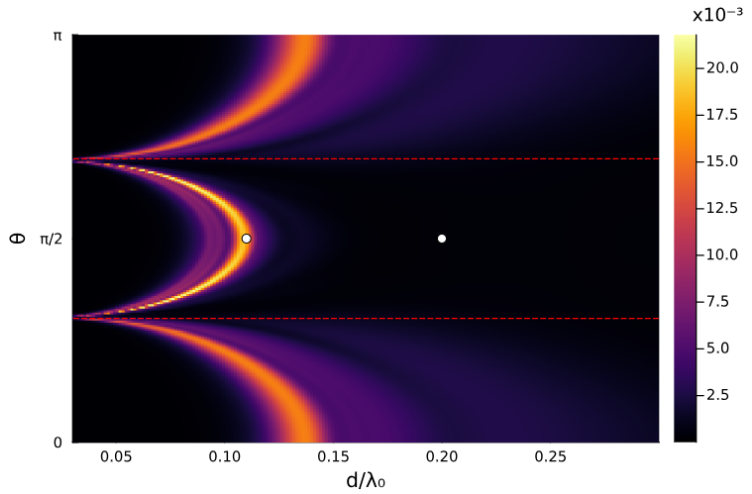

(a)

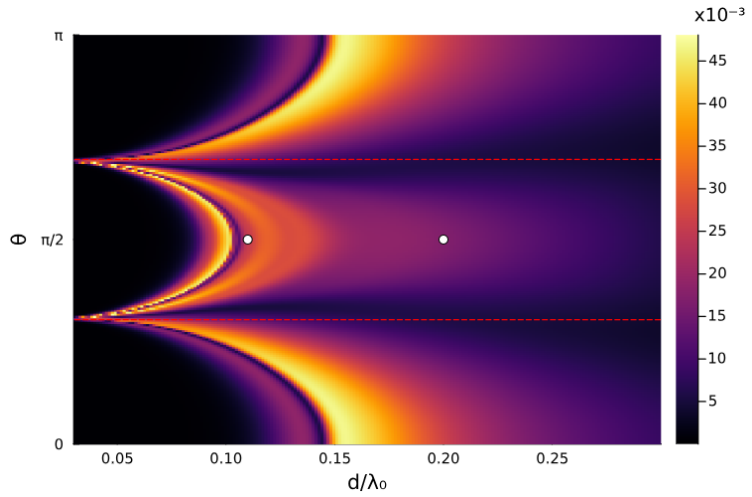

(b)

Figure 14: Shown is the NCBE between simulation results of the average excited state population for a chain of length 3 calculated in 2nd and 3rd order cumulant expansion in (a) and 1st and 3rd in (b) under variation of d and θ. The system is initially in the collective ground state and is driven with a constant pumping strength $\eta = \Gamma_0$. Note the error collapsing effect at the magic-angles(red dashed line). The white dots indicate parameter tuples for which the underlying time evolutions are shown exemplary in figure 17.

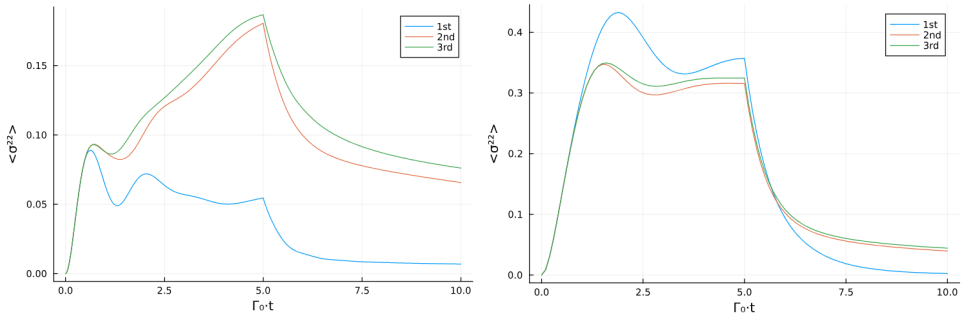

Figure 17: The time evolution corresponding to the marked white dots in figure 14 at $\theta = \frac{\pi}{2}$ and $d = 0.1$ on the left and $d = 0.2$ on the right. One sees, that very small changes in the systems density can provide huge impact on especially lower order correlations, changing the first order solution from finding equilibrium fast to having heavy perturbations in the case of a driven coupled ensemble.

3.6.2 Different pump functions

When looking at figure 13, but also figure 17, one probably noticed the sudden jumps at random positions. These irregularities are non-trivially linked to not just the pumping strength, but also the pumping type in a very unsystematic manner. Jumps happen more often when comparing higher order solutions. The following plot shows the NCBE for six different driving functions.

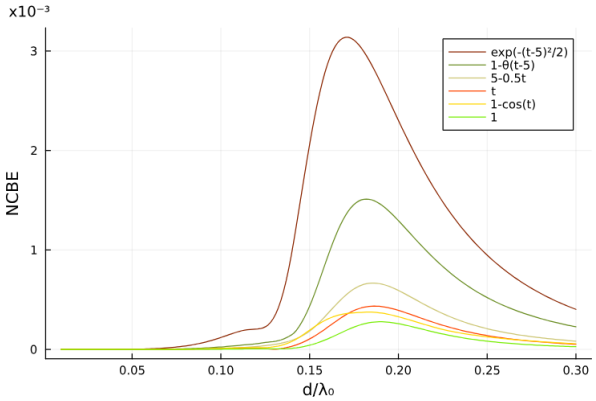

Figure 18: The NCBE for different inter-atomic spacings d when comparing average excited state population results in 2nd and 1st order while pumping with a variety of driving functions, as for example constant, gauss or linearly increasing pulses to show its impact on the jumps and total error. Distance is as always given in units of the transition wavelength ω_0.

Here in figure 18 the pumping functions $P_n(t)$ are normalized such, that $\int_0^{10} dt P_n(t) = 1$, where 0 and 10 denote the starting and end point in time of our simulation, to assure comparability amongst the protocols, so they all drive the system with the same total energy.

$$\begin{aligned} P_1(t) &= \frac{1}{\mathcal{N}} e^{-\frac{(t-5)^2}{2}} \\ P_2(t) &= \frac{1}{\mathcal{N}} (1 - \theta(t-5)) \\ P_3(t) &= \frac{1}{\mathcal{N}} (5 - 0.5t) \\ P_4(t) &= \frac{t}{\mathcal{N}} \\ P_5(t) &= \frac{1}{\mathcal{N}} (1 - cos(t)) \\ P_6(t) &= \frac{1}{\mathcal{N}} \end{aligned} \tag{52}$$

$\theta(t)$ denotes the Heaviside step function and $\mathcal{N}$ is a normalization constant.
When having normalized pump functions, former jumps disappear, so consequently jumps are linked to the normalization of a pump function and thus its amplitude, while the tail to the left of the peaks remains.

The key message of this plot however is that interestingly the errors amplitude is not just dependent on the pumping strength, but on the pumping type as well! The centered gauss pulse for example generates a nine times larger NCBE than the constant pulse at their peaks, while inserting the same amount of energy.
Finite rectangular and gaussian pulses seem to be especially unfavoured when performing cumulant expansions on correlation functions in driven systems.

To investigate how irregularities depend on the amount of energy inserted by the pump, we normalize the centered gaussian pulse to different values. One does not only see the already discussed shift towards smaller spacings with stronger pulses, but also that irregularities appear more often for larger energy transfers, characterized by jumps and dips. In this case adding roughly three to the value we normalize to generates one additional dip and the sudden jump to the left of the peaks shifts alongside the peak. The number of dipoles in the considered system by the way also enhances irregularities and their amount.

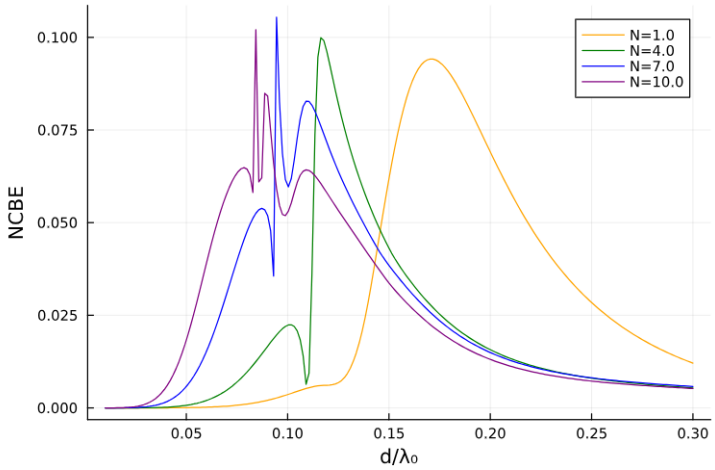

Figure 19: Plotted is the NCBE for two dipoles when varying their spacing, when they start in the collective ground state and get driven by a gaussian pulse centered at $\Gamma_0 \cdot t = 5$. The gaussian pulse, encoded in the pump function $P(t)$ in our hamiltonian, is normalized to different values, which corresponds to different energy transfers. The graphs are artificially scaled up such that their amplitudes are roughly equal to make differences in irregularities visible, as weaker pulses would induce less dynamics and thus logically lower absolute differences between different order solutions without any further value for interpretations.

3.6.3 Dynamics around error maxima

An obvious next step is to analyze how the peak position is related to the main competitors, being the coupling $\Omega_{ij}(d, \theta)$ and the pumping strength η, and how system dynamics change in its vicinity.

It was already mentioned in section 3.6, that one can use error maps in driven systems to look for parameter regimes, where quantum effects play a dominant role while having non-trivial and well observable system dynamics. Comparison between any orders can be utilized, but it is beneficial to compare to the first order cumulant expansion results for the largest deviations from the exact solution and hence error.

We will sweep through different driving powers and inter-atomic spacing to find said parameters and to plot maximum error curves.

We plotted the NCBE between different orders in figure 20 and found, that with a higher difference in orders the curve becomes steeper, meaning that the required pump power for generating the maximum increases significantly with increasing coupling strength.

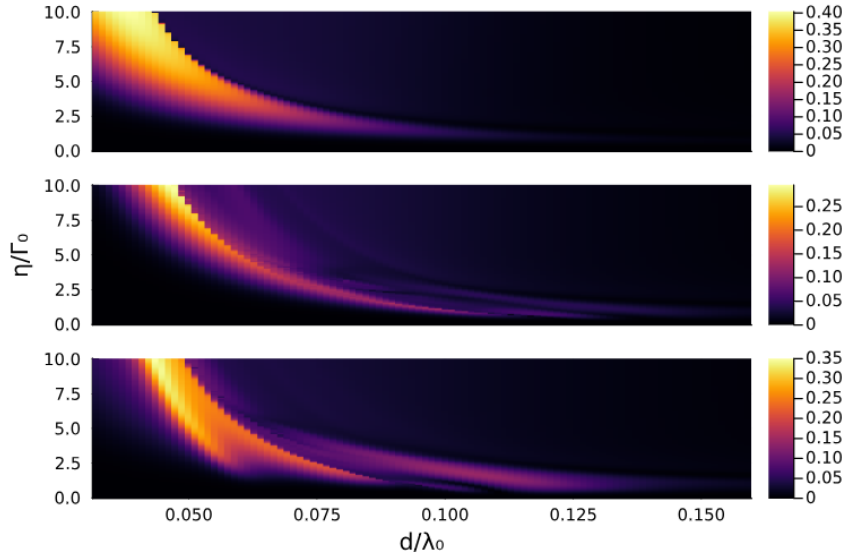

Figure 20: The NCBE between different orders cumulant expansion of the average upper state population in a chain of length four with transverse polarization is shown depending on pump strength and spacing, resembling the peak shift with increasing pump strength towards larger couplings. From top to bottom it is the NCBE stemming from the comparison between 2nd, 3rd and 4th to 1st order results.

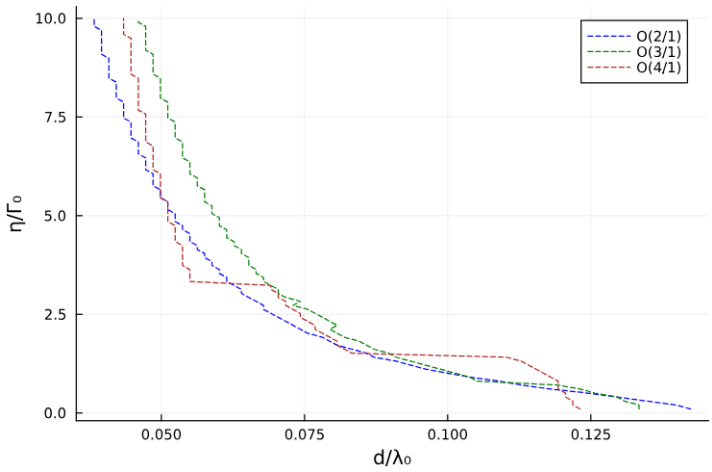

Figure 21: A plot, in which the 2D-plots in figure 20 were scanned for the parameters yielding the maximum error, i.e. the parameter tuples (d, η) yielding error peaks. For multiple η one or more time steps during the simulation cause instabilities, in which case the last function value arising from a stable solution is substituted, causing the graphs to have steps. For the $O(4/1)$-case we see two jumps between maximum error branches.

Where maxima occurred, one notices that this maximum-curve, especially visible in the case where exact and first order cumulant expanded solution are compared, can split into multiple branches.

The maximum error curve there shows two jumps between such branches in figure 21. Ergo it is possible to have multiple parameter tuples, which fit the rough description of being quantum mechanically and dynamically interesting and branches along stronger coupling fade faster when decreasing the driving strength.

But what actually happens in terms of time evolution at and around the peaks? To reply to this we plot the time evolution of the average excited state population expectation value for four configurations.

To the left of the maximum peak, the strong coupling locks the system to the ground state and prevents high population of the excited state, yielding low error capabilities. On both left branches the excited state population converges similarly and is drastically higher than in the first case and for $d = 0.082\lambda_0$ we see something we will observe more often later on, namely that with lower coupling of the quantum emitters, the excited state population converges faster towards its equilibrium determined by drive and coupling, at least for our considered systems. It is then more successfully approximated by a mean-field approach.

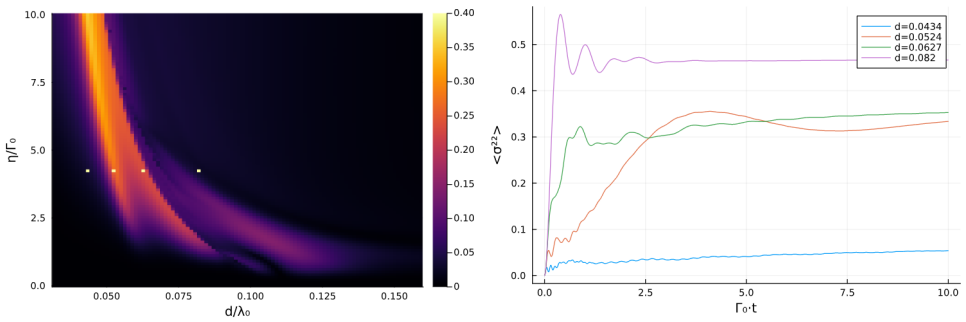

Figure 24: Shown is the NCBE when comparing 4th and 1st order solutions for $\langle\sigma^{22}\rangle(t)$ dependent on d and θ just like in figure 20 with four marked spots at $\eta = 4.\overline{24}$ and four distances specified in the plot labels on the left in units of the transition wavelength λ_0 and exact solutions for the time evolution of $\langle\sigma^{22}\rangle$ corresponding to these parameters on the right, having transversely polarized atoms.

To sum the recent chapters up: the total error dynamics is determined by the competition between higher and lower order correlations as well as drops due to zero-crossings and driving type and strength induced jumps, exhibiting interesting phase-like behaviour for the performance of different orders of cumulant expansion.

All these considerations are generalizable to any hamiltonian and thus system. One just needs to interchange the upcoming parameters.

3.7 Validity dependent on atom number

As the cumulant expansion in the context of this thesis is primarily meant to give access to information about the dynamics in very large systems, the system size is probably the most important parameter to consider when estimating its performance. To do so again the average upper state population in a chain of length N = 2 to 6 was simulated for an atomic spacing of $0.1\lambda_0$ and a tangential polarization of all atoms, starting in the collective ground state and constantly pumping with $\eta = \Gamma_0$ until $t = \frac{5}{\Gamma_0}$. This simulation was performed in all orders up to the system size N and the NCBE was calculated between all of these orders. The results are shown in table 1 below and the time evolutions, which are compared here, are shown in figure 25.

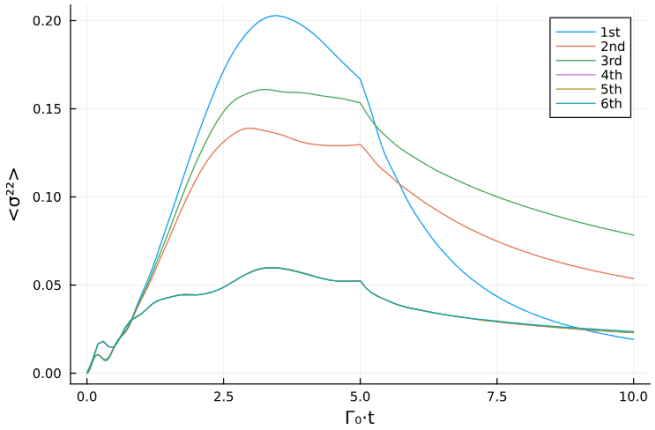

Figure 25: Average upper state population of all atoms, given by $\frac{1}{N}\sum_i^N \sigma_i^{22}$ with N=6 the number of atoms for the chain geometry in all six orders, showing significant improvement only from the 4th order on. However 2nd and 3rd order already exhibit the characteristic very slow decay compared to the purely exponential drop in 1st order.

Table 1: NCBE between different orders with NCBE(N,i) denoting the NCBE between exact and i-th order cumulant expanded solution for the chain geometry.

N	**6**$[10^{-2}]$	**5**$[10^{-2}]$	**4**$[10^{-2}]$	**3**$[10^{-2}]$	**2**$[10^{-2}]$
NCBE(N,N-1)	0.02069	0.03286	0.07847	0.26381	1.2151
NCBE(N,N-2)	0.02821	0.24155	0.78771	0.22751	
NCBE(N,N-3)	2.41013	0.58069	1.37152		
NCBE(N,N-4)	2.40548	0.74109			
NCBE(N,N-5)	2.43819				

In the first row the NCBE between exact solution, which can be interpreted as cumulant expansion up to Nth order, and solution in (N-1)th order is denoted by NCBE(N,N-1) and similarly the NCBEs between all orders for chains with N = 2 to 6 are covered.

Another geometry of interest is the ring, where every atom behaves perfectly alike due to its symmetry and thus the average dynamics of the average upper state population is given by $\frac{1}{N}\sum_i^N \langle\sigma_i^{22}\rangle = \langle\sigma_1^{22}\rangle = \langle\sigma_2^{22}\rangle = ...$

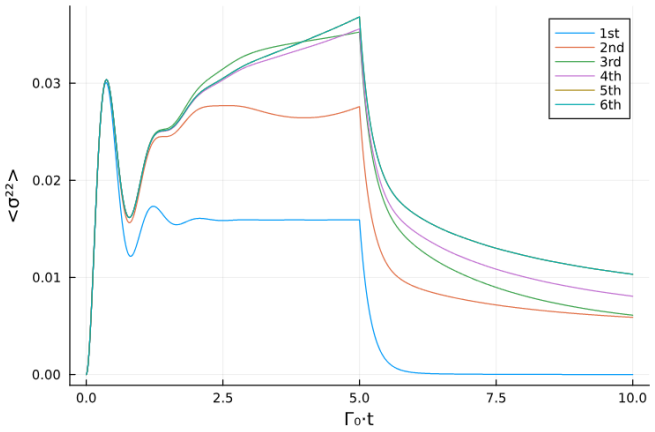

Figure 26: Shown is again the NCBE between all possible orders as in figure 25 but for the ring geometry, showing proper approximated results from the 2nd order on already. Note, that the upper state population in mean-field approximation interestingly converges equilibrium significantly faster than any other order.

Table 2: NCBE between different orders for the ring geometry, following the notation from table 1.

N	**6**$[10^{-2}]$	**5**$[10^{-2}]$	**4**$[10^{-2}]$	**3**$[10^{-2}]$	**2**$[10^{-2}]$
NCBE(N,N-1)	0.0107	0.04724	0.04896	0.11938	2.40246
NCBE(N,N-2)	0.11974	0.06131	0.04911	0.33015	
NCBE(N,N-3)	0.21093	0.52724	0.12507		
NCBE(N,N-4)	0.49927	0.65213			
NCBE(N,N-5)	1.31343				

Although an improvement with increasing system size could have been expected for each geometry, since under constant density every atom one would add to the system contributes less and less to the interaction terms and therefore neglecting correlations between these atoms should get more and more viable, there is sadly no pattern recognizable for either geometry and the performance also does not generally improve with larger system sizes, as demonstrated in figure 25 for the third order cumulant expansion for $N = 6$. It is just a tendency.

The discrepancy of the third order result from the exact solution in the chain-case may be connected to findings of the university of Strathclyde, Glasgow [14]. It was shown, that odd cumulants can have wrong convergence for $N \to \infty$, consequently resulting in ever larger deviations when increasing the system size for very similar models. Very well possible, that a chain of length six in our model is sufficiently large already to observe this effect, but for confirmation one would have to investigate more in its $N \to \infty$ scaling.

However it is remarkable, that fourth and fifth order cumulant expansion results in the case of the $N = 6$ - chain are almost indistinguishable from the exact solution by eye with exceptional NCBE's of the order of 10^{-4}. Overall though it turns out that compared to the chain the dynamics of quantum emitters arranged in a ring structure suffer less from an approximation via cumulant expansion.
As a side note the results improve for shorter and get insignificantly worse for longer simulation times. The former can be seen by eye already in both plots. However reducing simulation times piece-meal and add up the subdivided simulations is not a valid approach, as the simulation times have to be at least as long as the inverse decay rate of the most subradiant state or its impact on the system dynamics is not captured. A simulation over a time span of $\frac{1}{\Gamma_0}$ for example logically ignores anything subradiance related.

To sum it up using the fastest order to simulate without losing correlations between atoms, the 2nd order, already displays promising NCBE's of the order of 10^{-2}. And remember, this holds for a spacing of $0.1\lambda_0$, so for quite dense quantum systems, and since the approximation improves almost continuously for larger spacings, a motivation for the cumulant expansion used in any less dense system is given. It is particularly useful when solving combinatorial problems with an easy to check solution with discrete outcome where a rough solution is easy to correct such as the N-Queens problem for example.

4 Analytical cumulant expansion in 1st and 2nd order for two coupled nano-emitters

Analytical solutions have a variety of advantages over simulated ones.
For example they provide exact solutions without the approximations or discretizations inherent in numerical simulations, while being more comprehensible and might even reveal fundamental behaviours and dependencies that might be less apparent in numerical solutions as well as can lead to generalized insights that can apply to a broader range of systems.
This being said, we seek in this chapter for the analytical solution of a simple undriven two-dipole system, perform the cumulant expansion on it, generate an analytically derived NCBE error map and talk about the usage of the comparison between any order with the first order cumulants for investigations regarding the limits between classical and quantum physics.

4.1 Analytic solutions for a two-dipole system

A good performance of the cumulant expansion relies on higher order correlation terms being way smaller than their lower order expectation value counterparts, in best case negligible. Typically higher order correlation terms are expected to have less influence, as coupling decreases with distance.
The lower impact of higher order correlations and hence the difference between the orders is demonstrated by solving a system consisting of two coupled two-level atoms analytically for 1st and 2nd order cumulant expansion, having initially the first atom in the excited and the second in the ground state.
The starting point is the modified Quantum Langevin equation without white noise for the expectation value of an arbitrary operator O.

$$\langle \dot{O} \rangle = \frac{i}{\hbar} \langle [H, O] \rangle + \sum_{ij} \Gamma_{ij} \langle (\sigma_j^+ O \sigma_i^- - \frac{1}{2} \{ \sigma_i^+ \sigma_j^-, O \}) \rangle \tag{53}$$

Using equation 53 for e.g. the excited state population of the first atom $\langle \sigma_1^{22} \rangle$ leads to a differential equation dependent on other expectation values, which have to be solved as well, finally resulting in a closed system of four coupled differential equations:

$$
\begin{aligned}
\dot{A}_1(t) = \frac{d}{dt}\langle\sigma_1^{22}\rangle \quad &= -i\Omega_{12}\langle\sigma_1^{21}\sigma_2^{12}\rangle + i\Omega_{21}\langle\sigma_1^{12}\sigma_2^{21}\rangle \\
&\quad - \Gamma_{11}\langle\sigma_1^{22}\rangle - \frac{\Gamma_{12}}{2}\langle\sigma_1^{21}\sigma_2^{12}\rangle - \frac{\Gamma_{21}}{2}\langle\sigma_1^{12}\sigma_2^{21}\rangle \\
\dot{B}_1(t) = \frac{d}{dt}\langle\sigma_1^{21}\sigma_2^{12}\rangle \quad &= i\Omega_{12}\langle\sigma_2^{22}\rangle - i\Omega_{21}\langle\sigma_1^{22}\rangle - \frac{\Gamma_{11}}{2}\langle\sigma_1^{21}\sigma_2^{12}\rangle \\
&\quad + \Gamma_{21}(2\langle\sigma_1^{22}\sigma_2^{22}\rangle - \frac{1}{2}\langle\sigma_1^{22}\rangle - \frac{1}{2}\langle\sigma_2^{22}\rangle) - \frac{\Gamma_{22}}{2}\langle\sigma_1^{21}\sigma_2^{12}\rangle \\
\dot{A}_2(t) = \frac{d}{dt}\langle\sigma_2^{22}\rangle \quad &= i\Omega_{12}\langle\sigma_1^{21}\sigma_2^{12}\rangle - i\Omega_{21}\langle\sigma_1^{12}\sigma_2^{21}\rangle \\
&\quad - \frac{\Gamma_{12}}{2}\langle\sigma_1^{21}\sigma_2^{12}\rangle - \frac{\Gamma_{21}}{2}\langle\sigma_1^{12}\sigma_2^{21}\rangle - \Gamma_{22}\langle\sigma_2^{22}\rangle \\
\dot{B}_2(t) = \frac{d}{dt}\langle\sigma_1^{22}\sigma_2^{22}\rangle \quad &= -\Gamma_{11}\langle\sigma_1^{22}\sigma_2^{22}\rangle - \Gamma_{22}\langle\sigma_1^{22}\sigma_2^{22}\rangle
\end{aligned}
\tag{54}
$$

Latin letters will generally denote complex functions of time $f : \mathbb{C} \to \mathbb{C}$.

Technically it is also necessary to solve $\langle\sigma_1^{21}\sigma_2^{12}\rangle$, but swapping the direction indices in the jump operators around is trivially given by $\langle\sigma_1^{21}\sigma_2^{12}\rangle = \langle\sigma_1^{12}\sigma_2^{21}\rangle^\dagger$, since the general relation $\sigma_k^{ij} = (\sigma_k^{ji})^\dagger$ with $i, j, k \in \mathbb{N}$ holds, immediately observable when constructing the corresponding e.o.m. This also means, that $A_{1/2}(t)$ are hermitian and thus real.

Further the equations can be simplified under consideration of the symmetries of the two-atom-system by setting $\Gamma_{11} = \Gamma_{22} = \Gamma_0$, $\Omega_{21} = \Omega_{12} = \Omega$, $\Gamma_{12} = \Gamma_{21}$ and renaming the operator expectation values as shown in equation 54.

$$
\begin{aligned}
\dot{A}_1(t) &= -\Gamma_0 A_1(t) + i\Omega(B_1^\dagger(t) - B_1(t)) - \frac{\Gamma_{12}}{2}(B_1(t) + B_1^\dagger(t)) \\
\dot{B}_1(t) &= -\Gamma_0 B_1(t) + (-i\Omega - \frac{\Gamma_{12}}{2})A_1(t) + (i\Omega - \frac{\Gamma_{12}}{2})A_2(t) - 2\Gamma_{12}B_2(t) \\
\dot{A}_2(t) &= -\Gamma_0 A_2(t) + i\Omega(B_1(t) - B_1^\dagger(t)) - \frac{\Gamma_{12}}{2}(B_1(t) + B_1^\dagger(t)) \\
\dot{B}_2(t) &= -2\Gamma_0 B_2(t)
\end{aligned}
\tag{55}
$$

There seems to be no direct way of solving this equation, so the first step will be to prematurely cancel out $B_2(t) = 0$ by transforming the equations such that

$$
\begin{bmatrix} A_1^*(t) \\ A_2^*(t) \\ B_1^*(t) \\ B_2^*(t) \end{bmatrix} = \begin{bmatrix} 1 & 0 & 1 & 0 \\ 0 & 1 & 1 & 0 \\ 0 & 1 & 1 & 0 \\ 0 & 0 & 0 & 0 \end{bmatrix} \begin{bmatrix} A_1(t) \\ A_2(t) \\ B_1(t) \\ B_2(t) \end{bmatrix}
\tag{56}
$$

Doing so will neglect the crucial interaction part or in other words the effect of the real part of $B_1(t)$ on $A_1(t)$ and $A_2(t)$, leading to a fully symmetric coupled differential equation and it is valid since $-\Gamma_{12}B_2(t)$ will only generate an additive term in the solution for $B_1(t)$.

This step is related to a basis change from an individual to a collective basis.
This allows us to later on use a simplification, as we know already one part of $A_{1/2}(t)$ and the imaginary part of $B_1(t)$, which is the same as the imaginary part of $A^*_{1/2}(t)$, since $A_1(t)$ and $A_2(t)$ are real functions $A_{1/2}(t) : \mathbb{R} \to \mathbb{R}$.
As $B_1(t)$ is a function with complex values and for a complex number $\alpha \in \mathbb{C}$ applies $\alpha+\alpha^\dagger = 2\Re(\alpha)$ and $\alpha - \alpha^\dagger = 2i\Im(\alpha)$, this also applies to the function itself.

$$\begin{aligned}
\dot{A}^*_1(t) &= -\Gamma_0 A^*_1(t) - 2i\Omega\Im(B^*_1(t)) - \Gamma_{12}\Re(B^*_1(t)) \\
\dot{B}^*_1(t) &= -\Gamma_0 B^*_1(t) + (-i\Omega - \frac{\Gamma_{12}}{2})A^*_1(t) + (i\Omega - \frac{\Gamma_{12}}{2})A^*_2(t) \\
\dot{A}^*_2(t) &= -\Gamma_0 A^*_2(t) + 2i\Omega\Im(B^*_1(t)) - \Gamma_{12}\Re(B^*_1(t))
\end{aligned} \tag{57}$$

As a side note one equation is technically redundant. The symmetry between $A_1(t)$ and $B_1(t)$ implies, that $A^*_1(t) = B^*_1(t)$ as well as $A^*_2(t) = (B^*_1)^\dagger(t)$, yielding a trivially solvable first order differential equation.

$$\dot{A}^*_1(t) = -\Gamma_0 A^*_1(t) - 2i\Omega\Im(A^*_1(t)) - \Gamma_{12}\Re(A^*_1(t)) \tag{58}$$

Thus the composite solutions considering the initial conditions read:

$$\begin{aligned}
A^*_1(t) &= e^{-\Gamma_0 t}\left(\frac{1}{2}e^{-2i\Omega t} + \frac{1}{2}e^{-\Gamma_{12}t}\right) \\
A^*_2(t) &= e^{-\Gamma_0 t}\left(-\frac{1}{2}e^{-2i\Omega t} + \frac{1}{2}e^{-\Gamma_{12}t}\right) \\
\Im(B^*_1(t)) &= \Im(B_1(t)) = e^{-\Gamma_0 t}\left(-\frac{1}{2}sin(2\Omega t)\right)
\end{aligned} \tag{59}$$

The next step is to find the real part of $B_1(t)$. The strategy here is to simplify equations 55 by modifying $A^{'}_1(t) = e^{\Gamma_0 t}A_1(t)$ for all expectation values, since the prefactor $e^{-\Gamma_0 t}$ occurs in all equations, yielding a set of coupled equations, which don't depend on their function themselves anymore, allowing to take the time derivative of the equation for $B^{'}_1$ and construct a second order differential equation by plugging in $\dot{A}^{'}_1(t)$ and $\dot{A}^{'}_2(t)$.

$$\begin{aligned}
\ddot{B}^{'}_1(t) &= (-i\Omega - \frac{\Gamma_{12}}{2})\dot{A}^{'}_1(t) + (i\Omega - \frac{\Gamma_{12}}{2})\dot{A}^{'}_2(t) - \Gamma_{12}\dot{B}^{'}_2(t) \\
&= (-i\Omega - \frac{\Gamma_{12}}{2})[-i\Omega(B^{'}_1(t) - B^{'\dagger}_1(t)) - \Gamma_{12}(B^{'}_1(t) + B^{'\dagger}_1(t))] \\
&\quad + (i\Omega - \frac{\Gamma_{12}}{2})[i\Omega(B^{'}_1(t) - B^{'\dagger}_1(t)) - \Gamma_{12}(B^{'}_1(t) + B^{'\dagger}_1(t))] - \Gamma_{12}\dot{B}^{'}_2(t) \\
&= 2i\Omega^2 \sin(2\Omega t) + \Gamma^2_{12}\Re(B^{'}_1(t)) - \Gamma_{12}\dot{B}^{'}_2(t)
\end{aligned} \tag{60}$$

The imaginary part has been solved already and we are only interested in the real part by now. Apart of that, luckily the equation for $B_2(t)$ is trivially solved by $B_2^{'}(t) = e^{-\Gamma_0 t}$ and thus we obtain an easy inhomogeneous second order differential equation for the real part of $B_1^{'}(t)$.

$$\Re(\ddot{B}_1^{'}(t)) - \Gamma_{12}\Re(B_1^{'}(t)) = \Gamma_{12}\Gamma_0 e^{-\Gamma_0 t} \tag{61}$$

This can be solved by performing the sum of homogeneous and particular solution, using the variation of constants method with the given initial conditions, leading to $\Re(B_1(t))$ after back transformation and thus the final result for $B_1(t)$.

$$\Re(B_1(t)) = e^{-\Gamma_0 t}\Re(B_1^{'}(t)) = \frac{1}{4}\left(-e^{-(\Gamma_0-\Gamma_{12})t} + e^{-2\Gamma_0 t}\right) \tag{62}$$

The final solutions for the coupled differential equations 55 are hence:

$$\begin{aligned}
A_1(t) &= \langle\sigma_1^{22}\rangle = e^{-\Gamma_0 t}\left(\frac{1}{2}cos(2\Omega t) + \frac{1}{2}e^{-\Gamma_{12}t}\right) - \frac{1}{4}\left(-e^{-(\Gamma_0-\Gamma_{12})t} + e^{-2\Gamma_0 t}\right)\\
A_2(t) &= \langle\sigma_2^{22}\rangle = e^{-\Gamma_0 t}\left(-\frac{1}{2}cos(2\Omega t) + \frac{1}{2}e^{-\Gamma_{12}t}\right) - \frac{1}{4}\left(-e^{-(\Gamma_0-\Gamma_{12})t} + e^{-2\Gamma_0 t}\right)\\
B_1(t) &= \langle\sigma_1^{21}\sigma_2^{12}\rangle = \frac{i}{2}e^{-\Gamma_0 t}sin(-2\Omega t) + \frac{1}{4}\left(-e^{-(\Gamma_0-\Gamma_{12})t} + e^{-2\Gamma_0 t}\right)\\
B_2(t) &= \langle\sigma_1^{22}\sigma_2^{22}\rangle = 0
\end{aligned} \tag{63}$$

These are the exact solutions, clearly showing the lower impact of the higher order correlation term $B_1(t)$ on the overall dynamic compared to the single operator terms by simply being smaller. $B_1(t)$ being negative also means, that $A_1(t)$ is less steep than a classical counter part indicating subradiance, as we will see in a bit.

The fourth equation $\dot{B}_2(t) = -2\Gamma_0 B_2(t)$ also turns out to be in agreement with observations by Laurin Ostermann stating, that the totally inverted state $|e\rangle$ with all N atoms in the excited state decays with a collective emission rate $\Gamma_e = \sum_i^N \Gamma_0 = N\Gamma_0$, completely independent on the geometry. In our case $N = 2$ and thus $B_2(t) = e^{-2\Gamma_0 t}$[13].

Noteworthy is the characteristic extremely slow decay for longer times and the decaying oscillations of the upper state populations for first and second dipole, with a phase shift of $-\frac{\pi}{2}$, resembling the continuous photon exchange between the two dipoles under presence of dissipation.

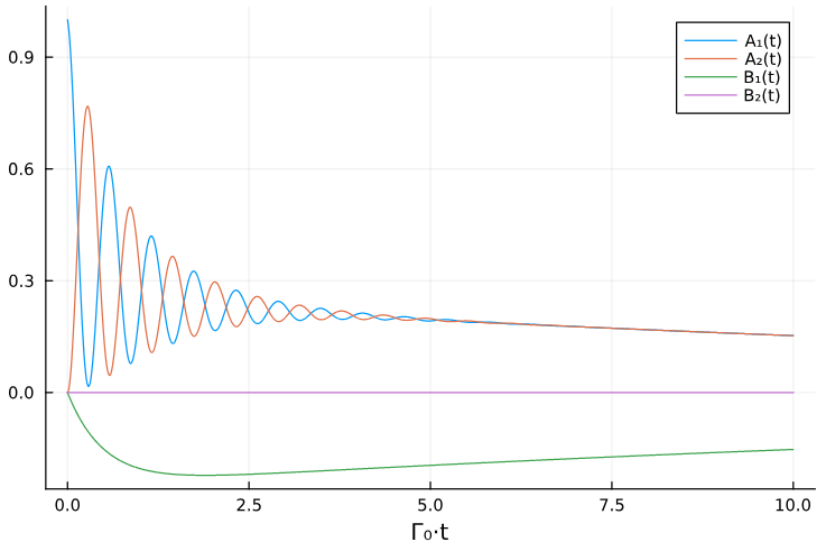

Figure 27: Plot of the real part analytic solutions shown in equation 63, visualizing the modifying effect of the second order term $B_1(t)$ on the systems dynamics. The chosen parameters are $\Omega = 5.38$, $\theta = \frac{\pi}{2}$, $\Gamma_0 = 1.0$ and $\Gamma_{12} = 0.95$.

Now lets see how the e.o.m. look like after performing the first order cumulant expansion on $\langle \sigma_1^{22} \rangle = a_1(t)$ using equation 43 and complete the set of equations by solving further occuring expectation values again.

$$
\begin{aligned}
\frac{d}{dt}\langle \sigma_1^{22} \rangle = \dot{a}_1(t) =& -\Gamma_0 a_1(t) - i\Omega(b_1(t)b_2(t) - b_1^\dagger(t)b_2^\dagger(t)) \\
& - \frac{\Gamma_{12}}{2}(b_1(t)b_2(t) + b_1^\dagger(t)b_2^\dagger(t)) \\
\frac{d}{dt}\langle \sigma_2^{22} \rangle = \dot{a}_2(t) =& -\Gamma_0 a_2(t) + i\Omega(b_1(t)b_2(t) - b_1^\dagger(t)b_2^\dagger(t)) \\
& - \frac{\Gamma_{12}}{2}(b_1(t)b_2(t) + b_1^\dagger(t)b_2^\dagger(t)) \\
\frac{d}{dt}\langle \sigma_1^{21} \rangle = \dot{b}_1(t) =& (-\Gamma_0 + i\omega)b_1(t) + i\Omega(b_2^\dagger(t) - 2a_1(t)b_2^\dagger(t)) \\
& - \frac{\Gamma_{12}}{2}(b_2^\dagger(t) - 2a_1(t)b_2^\dagger(t)) \\
\frac{d}{dt}\langle \sigma_2^{12} \rangle = \dot{b}_2(t) =& (-\frac{\Gamma_0}{2} - i\omega)b_2(t) + i\Omega(b_1^\dagger(t) - 2a_2(t)b_1^\dagger(t)) \\
& - \frac{\Gamma_{12}}{2}(b_1^\dagger(t) - 2a_2 b_1^\dagger(t))
\end{aligned}
\tag{64}
$$

This still looks complicated on first sight, but since the prefactors of the expressions $a_i(t), b_j(t)$ with $i, j \in 1, 2$, stemming from the self repeating terms, differ already and the imaginary part is not generally vanishing in $a_i(t)$, the only valid solution is extremely simple.

$$\begin{aligned} a_1(t) &= e^{-\Gamma_0 t} \\ a_2(t) = b_1(t) &= b_2(t) = 0 \end{aligned} \tag{65}$$

This analytical solution substantiates the first order describing a system under consideration classical, as it resembles a completely uncoupled system, where the first atom decays on its own with the characteristic decay rate Γ_0 while the second atom is not influenced at all and will hence stay in the ground state forever, i.e. no photons are exchanged.

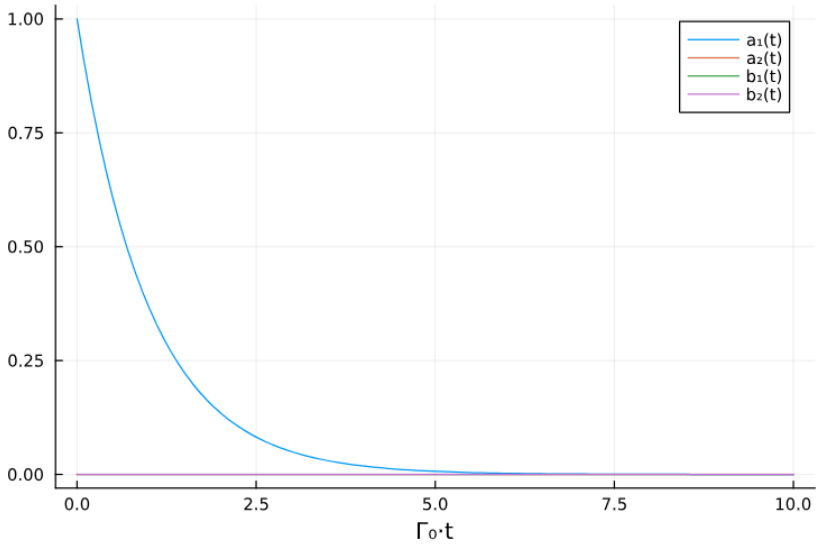

Figure 28: Plot of the analytic solutions for the operator expectation values appearing in the coupled differential equation described in equation 54 as in figure 28 but after performing the first order cumulant expansion to σ_1^{22} in equation 63, showing independent atoms.

Apart of the vanishing correlation between the excited state populations carrying $B_2(t)$ term and thus the symmetry breaking between the e.o.m. for $A_{1/2}(t)$ and $B_1(t)$, the main reason the system collapses mathematically to the classical solution is due to the expectation values of the first order jump operators immediately leading to unphysical behaviour, i.e. not fulfilling the initial conditions without being trivial.

When going down in orders, only the dominating envelope, in our case $e^{-\Gamma_0 t}$, remains, so the general tendency in the non-driven dissipative system $\lim_{t\to\infty}\langle\sigma_i^{22}(t)\rangle = 0$ still holds, respectively the boundary conditions have to match, but detailed dynamics mainly captured by terms containing Ω and Γ_{12} are discarded. Ergo mean-field approaches are specifically useful in the context of limit considerations.

The difference between the upper state population expectation value time derivatives in neighbouring orders corresponds by the way to well known statistical measures. The difference between order one and two for example is a weighted sum of variances of ladder operators and thus the error maps using the NCBE are linked to them as well.

$$\begin{aligned}\langle\dot{\sigma_1^{22}}\rangle_{\mathcal{O}2} - \langle\dot{\sigma_1^{22}}\rangle_{\mathcal{O}1} &= (i\Omega - \frac{\Gamma_{12}}{2})\mathcal{V}(\sigma_1^{12}\sigma_2^{21}) + (-i\Omega - \frac{\Gamma_{12}}{2})\mathcal{V}(\sigma_1^{21}\sigma_2^{12}) \\ &= \Omega e^{-\Gamma_0 t} sin(2\Omega t) - \frac{\Gamma_{12}}{4}\left(-e^{-(\Gamma_0-\Gamma_{12})t} + e^{-2\Gamma_0 t}\right)\end{aligned} \tag{66}$$

$\mathcal{V}(\mathbf{X})$ denotes the variance of $\mathbf{X}$.

First order terms logically vanish, there is no difference in the beginning and for $t \to \infty$ and it oscillates with the same frequency as operator expectation values 2Ω.

4.2 Analytic error

After having solved the problem of two dipoles exchanging photons and slowly decaying, we can analyze the error quantity we used for simulations, i.e. the NCBE [50], in more detail to gain information about which irregularities and behaviours in general stem from numerical origins like rounding errors for example and which from the cumulant expansion and the error measure itself.

To this end a heatmap in analogy to figure 9 is created but using the analytic results.

Following the definition of the NCBE we obtain a formula for this particular case.

$$\begin{aligned}\text{NCBE} &= \frac{1}{N}\sum_{n=1}^{N}|A_1(t_n) - a_1(t_n)| \\ &= \frac{1}{N}\sum_{n=1}^{N}\Bigg|e^{-\Gamma_0 t_n}\left(\frac{1}{2}\cos(2\Omega t_n) + \frac{1}{2}e^{-\Gamma_{12}t_n} - 1\right) \\ &\quad - \frac{1}{4}\left(-e^{-(\Gamma_0-\Gamma_{12})t_n} + e^{-2\Gamma_0 t_n}\right)\Bigg|\end{aligned} \tag{67}$$

$t_n \in [t_1, t_N]$ denotes the time step at time bin n and N is the total amount of bins.

What we see are the outer lines roughly following the zero-crossing of $\Omega(\theta, d)$ and special behaviour at the magic angles. Multiple things are surprising though.

First of all we see irregular peaks everywhere in the very dense regime behind the outer lines, occuring as yellow dots, symmetrically distributed with respect to the dipole polarizations θ. This ultimately means, that the peaks also shown in simulation results, for example in 19, are no numerical errors, but one can show by increasing the time span, that the dots and rings in the high density regime are flattened out and are caused to converge towards the shape of a similar error heatmap for two excited dipoles as we saw in figure 9.

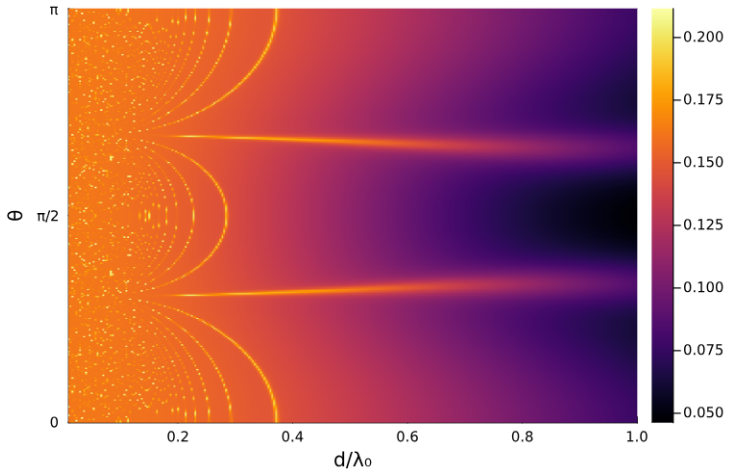

Figure 29: Analytic error map based on the NCBE between $A_1(t)$ and $a_1(t)$, i.e. 2nd and 1st order cumulant expansion of the expectation value of operator σ_1^{22}. The functions at each point were evaluated over a time span of $\Gamma_0 \cdot t \in [0, 10]$.

This is linked to oscillations at early times, whose frequency varies with Ω and will cause significant changes due to the nature of the NCBE. So the rings denote excited state population expectation values of constant frequency $\Omega(d, \theta)$, which lead to high deviation between different orders. One can flatten the rings by simulating over infinite times. Thus also the peaks in former error maps would be smooth for an infinite amount of time steps.

Second the error at the magic angles does not exhibit a minimum, but a peak instead. At the magic angles the coupling Ω vanishes and for a large range of d holds $\Gamma_{12} \approx \Gamma_0$, so $\langle\sigma_1^{22}\rangle(t)$ converges to $\frac{1}{4}$, since

$$\begin{aligned}\lim_{\Omega\to 0,\Gamma_{12}\to\Gamma_0}\langle\sigma_1^{22}\rangle(t) = \lim_{\Omega\to 0,\Gamma_{12}\to\Gamma_0}&\left[e^{-\Gamma_0 t}\left(\frac{1}{2}cos(2\Omega t)+\frac{1}{2}e^{-\Gamma_{12}t}\right)\right.\\ &\left.-\frac{1}{4}\left(-e^{-(\Gamma_0-\Gamma_{12})t}+e^{-2\Gamma_0 t}\right)\right]\\ &= e^{-\Gamma_0 t}\left(\frac{1}{2}+\frac{1}{2}e^{-\Gamma_0}\right)-\frac{1}{4}\left(-e^0+e^{-\Gamma_0 t}\right)\end{aligned} \tag{68}$$

$$\Rightarrow \lim_{t\to\infty}\left[\lim_{\Omega\to 0,\Gamma_{12}\to\Gamma_0}\langle\sigma_1^{22}\rangle(t)\right]=\frac{1}{4}\,. \tag{69}$$

So since the decay for long times to zero is turned off for these specific angles, the cumulative error gets larger for long and consequently diverges for infinite times. It is therefore dependent on the system and its initial conditions, if an error peaks or dips at the magic angles. It is only certain, that a heavy deviation from its neighbouring environment on error maps will happen.

4.3 Limits to quantum effects in quantum optical systems of identical dipole ensembles

We saw already in the section 3.6 about driven systems, that the cumulant expansion method can be used for more than just approximations for quantum dynamics. Back then the comparison between different orders gave the possibility to track necessary density relative to a certain pumping strength to be able to detect dynamics.

Now, since the cumulant expansion up to first order correlation functions resembles a system under consideration classical, a comparison between an arbitrary order with the first one gives rise to investigations towards the correspondence principle and finding out more about the exact limits of classical and quantum physics.

That quantum effects become significant at the sub-wavelength regime is not strictly true. Comparisons between first and a different order cumulant expansion can be used to quantify this unprecise statement.

The simple case of two transversely polarized dipoles from section 4.1 already exhibits, that in fact differences between classical and quantum behaviour are not mainly captured by the systems density, but by its coupling parameters, as $\sigma_1^{22}(d=0.5\lambda_0,t)$ is already reasonably insignificant due to the zero-crossing of the coupling at roughly this distance. In fact the NCBE between second and first order solution for $\sigma_1^{22}(t)$ is about 0.01 for $\frac{d}{\lambda_0}=0.5,1.0$ and 2.0.

Using mean field comparison to sense for limits however works only, if the first order results really resemble a system under consideration classical. While this is largely correct for our nano-photonic arrays up to now, we will show a counterexample in the next section.

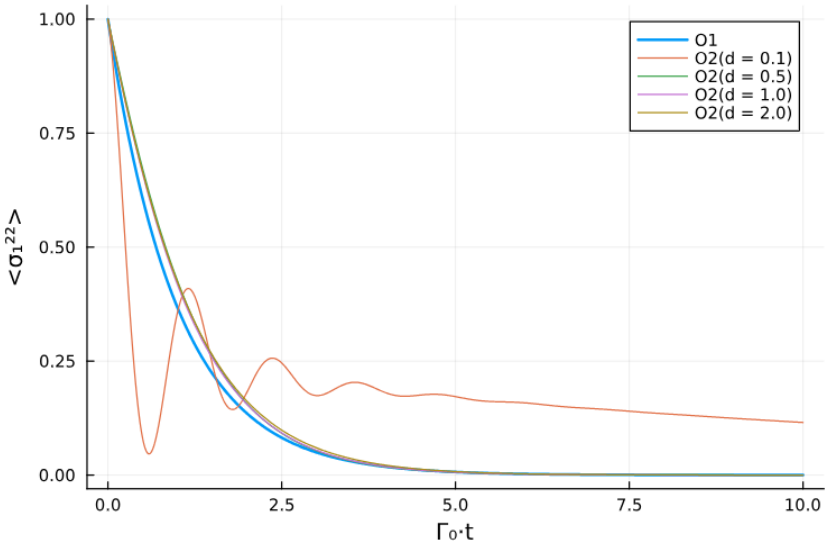

Figure 30: The excited state population in the first atom simulated for the system in 4.1 for different spacings d in units of the transition wavelength λ_0 and thus coupling between the dipoles. It shows insignificance of quantum effects even in the sub-wavelength regime, establishing, that the general assumption quantum effects get significant in the sub-wavelength regime is not true when coupling parameters with zero-crossings before $d = \lambda_0$ appear.

5 Example of a ring with antenna unit

In recent sections we could demonstrate exceptional performance of cumulant expansions on averages in typical quantum optical regimes, i.e. atom spacings of about $0.1\lambda_0 - 1.0\lambda_0$, exhibiting NCBE's around 10^{-2} and below. Thus we can confidently deduce system properties using cumulant expansion up to first and second order for similar systems.

We will stick to analyzing state populations in driven systems of $N-1$ identical coupled quantum emitters, arranged in a ring structure in the sub-wavelength regime, so this array of quantum emitters again exhibits sub- and superradiant behaviour.

Further we add an atom to the center of the ring, which acts as an absorptive impurity, so the ring behaves like a lens onto the central atom, which will lead to a highly efficient single photon antenna. Such a center can among other things enhance collective emission comparable to an iron core inside a magnetic coil, strengthening the magnetic flux.

This is a design motivated by LHC-molecules as in ref. [4,12], where energy is transported towards the impurity and then used by the reaction center. In this context we introduce a third auxiliary energy level, the target state for our antenna, and decay from the second to the third state inside an atom will correspond to local internal losses.

We use the same hamiltonian as in the preceding chapters resembling a constantly driven system of coupled quantum emitters.

$$H = \sum_{i}^{N} \omega \sigma_i^{22} + \sum_{i \neq j}^{N} \Omega_{ij} \sigma_i^{21} \sigma_j^{12} + \sum_{i}^{N} \eta(\sigma_i^{21} + \sigma_i^{12}) \tag{70}$$

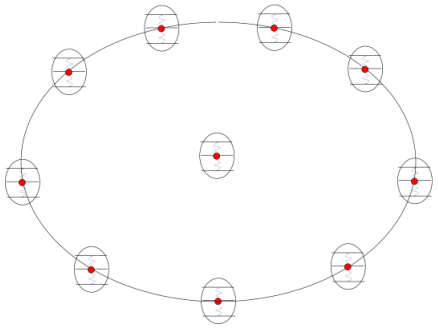

Figure 31: A sketch of the antenna ring containing nine identical quantum emitters and an impurity in the center. The atoms are equally distributed and have three energy levels. Decay to the third level corresponds to a local internal loss of excitation.

5.1 State population dynamics in 1st and 2nd order

A very similar antenna model has already been studied by Cardoner, Holzinger, Ritsch [12] and solved exactly with quite interesting results, as for example the appearance of an extreme dark state exactly for rings with $N = 9$ ring atoms.

Here we will derive operator dynamics computationally more efficient under utilization of the cumulant expansion with very little trade off. As a reminder the complexity of the problem is then reduced from something scaling exponentially with N to something with a polynomial scaling.

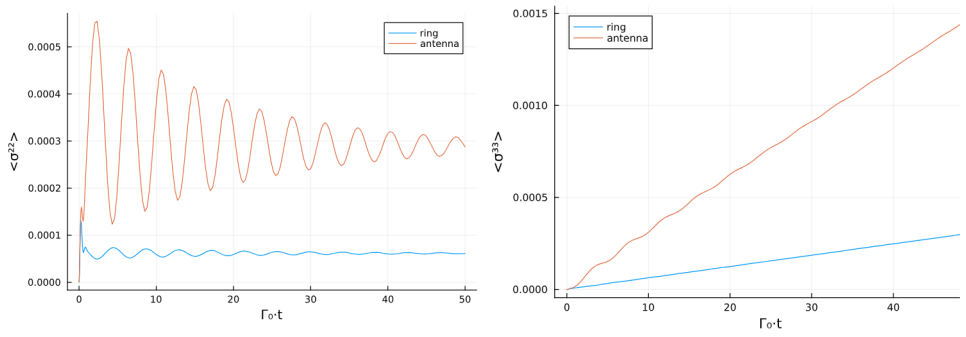

Figure 34: The time evolution of the expectation value of the excited state population in the second and the third energy level respectively for the antenna unit and a representative single ring element, as the ring is fully symmetric. We are in a very dense system with ring radius $R = 0.125\lambda_0$. The atoms polarization is circular, described by the vector $\vec{\mu} = \frac{1}{\sqrt{2}}(1 \ -i \ 0)^T$. We choose a small constant drive $\eta = 0.1\Gamma_0$ - set to be as large as the transition rate between the second and third level.

We observe, that the light from the pump laser charges up the system, causing rapid population of the second energy level in both, ring and antenna. The average population starts to oscillate around an equilibrium point due to drive and dissipation. The trigonometric functions describing ring element and antenna are shifted by π. We can interpret this as a light flux from the ring towards the antenna and as every ring element contributes, the antenna obviously gains a higher average.

When considering the average excited state population in the third energy level, we observe a seemingly linear charge up with a larger slope for the antenna unit compared to the ring constituents. We model our internal losses to be constant decay with rate $\Gamma_{23} = 0.1\Gamma_0$ and thus a higher excited state population expectation value causes higher population of the auxiliary state as well.

We can further quantify the antennas efficiency by defining and plotting the gain as ratio between the average state population in the center and the ring.

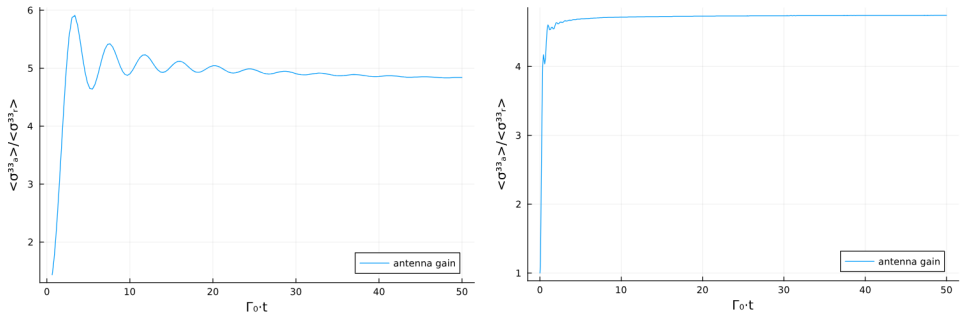

Figure 37: Plotted is the antenna gain, i.e. the ratio $\frac{\langle\sigma_a^{33}\rangle}{\langle\sigma_r^{33}\rangle}$ with $\langle\sigma_r^{33}\rangle = \frac{1}{N-1}\sum_i^{N-1}\langle\sigma_i^{33}\rangle$ for two different polarizations. If the ratio is positive, more energy is deposited in the reaction center than lost by the ring atoms and vice versa if it is negative. On the left for the ensemble with circular polarization described in figure 34 and on the right with tangential polarization with the center dipole pointing up the plane.

Clearly the simulation proves particular quality of the antennas storage ability, since the gain is much larger than one and it also seems to gain population in the auxiliary state faster, indicated by the early peak.
It is also favoured by an array of circular polarized dipoles compared to the case of tangentially polarized dipoles.
All of this information was obtained on an average laptop in less than twenty seconds.
We can also do the same for a ring of size $N = 18$ with a central impurity in an outstanding time of less than a minute of computation to find a gain way higher than just double the gain of the $N = 9$-ring.
For comparison calculating the $N = 18$ - ring in 2nd order cumulant expansion takes about 15 minutes and the exact solution can only be obtained in a reasonable amount of time by using high performance cluster computers. When using the cumulant expansion in the latter one can therefore probably even handle simulations with multiple hundreds of atoms involved.

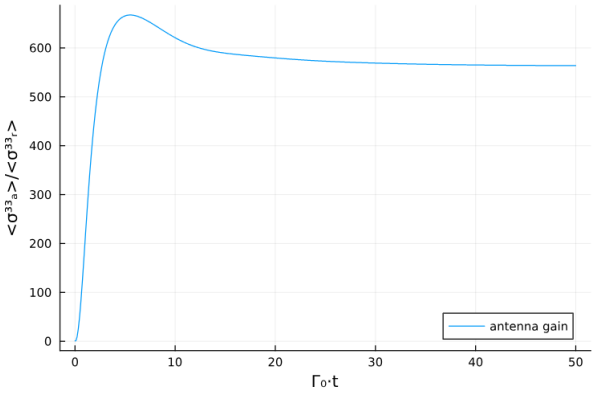

Figure 38: Plotted is again the gain of the ring in the antenna $\frac{\langle \sigma_a^{33} \rangle}{\langle \sigma_r^{33} \rangle}$ with the same aligned polarization as described in figure 34, but for $N = 18$ ring atoms.

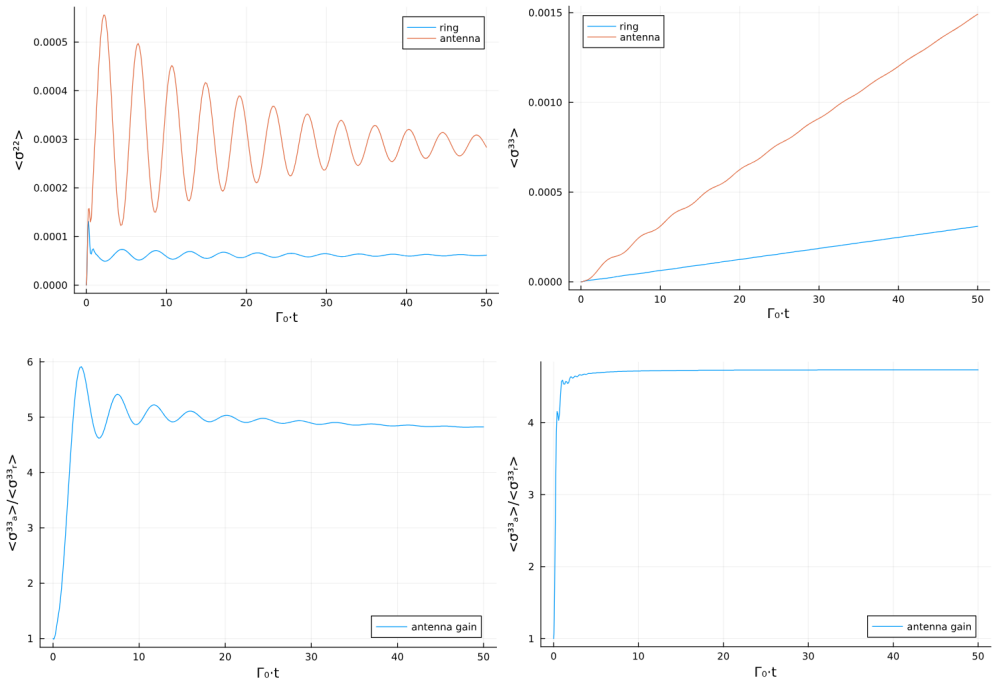

Figure 39: Second order results for the state population in ring and antenna in the second and third energy level and the ring gain for circular and tangential polarization, as shown for first order in figure 34 and 37.

The figures above show state populations and gain again, but this time simulated using second order cumulant expanded results. First order results are insignificantly worse than the second order ones with NCBE's of about $\sim 10^{-4}$ between each other. In fact one can without access to the exact solution not even know, if the second order results are better than the first order ones. Regardless the difference is minimal and the mean-field approximation succeeds in capturing physical results.

5.2 Enhanced dark state population using mean-field

Another example for successful use of a mean-field approach and an interesting observation in agreement with findings of Raphael Holzinger is an enhanced dark state population when partially irradiating the antenna ring. In section 5.1 all ten atoms were radiated with energy $\hbar\eta$ with light perpendicular to the dipole plane. Following this scheme, mainly the superradiant state $|\Psi_\mathrm{S}\rangle$ will be populated.

In our bio-inspired antenna however we want to mainly populate the subradiant state, i.e. the dark state $|\Psi_\mathrm{A}\rangle$, since less lost excitations to the environment correspond to a higher population of our target state σ_N^{33} due to the constant rate Γ_{23} in our model.

To achieve that one has to cause an asymmetry in the radiation of the atoms, either by changing the direction of the incoming light, so different atoms pick up different phases of the electric field, or by radiating the ring partially. When choosing the latter and e.g. only driving the first atom, i.e. the antenna, one can quantitatively show the enhancement of the dark state population by considering transition amplitudes when driving from the collective ground state $|G\rangle = |g\rangle^{\otimes N}$ to the super- and subradiant states. For simplicity we restrict ourselves to uncoupled atoms and the single-excitation manifold.

Following reference 15 the bright and dark state with one excitation reads

$$\begin{aligned} |\Psi_\mathrm{S}\rangle &= \frac{1}{\sqrt{N}}(\sigma_1^+ + \sqrt{N-1}S_2^+)|G\rangle \\ |\Psi_\mathrm{A}\rangle &= \frac{1}{\sqrt{N}}(\sqrt{N-1}\sigma_1^+ - S_2^+)|G\rangle \end{aligned} \tag{71}$$

where $S_2^+ = \frac{1}{\sqrt{N-1}}\sum_{j=2}^{N}\sigma_j^+$ is the collective ladder operator for the $N-1$ atoms in the outer ring with its complex conjugate S_2^-. Using these and our antenna driving hamiltonian $H_\mathrm{L} = \eta(\sigma_1^+ + \sigma_1^-)$ we can calculate transition amplitudes.

$$\begin{aligned} \langle\Psi_\mathrm{S}|H_\mathrm{L}|G\rangle &= \frac{1}{\sqrt{N}}\langle G|(\sigma_1^- + \sqrt{N-1}S_2^-)\eta(\sigma_1^+ + \sigma_1^-)|G\rangle \\ &= \frac{1}{\sqrt{N}}\left[\langle G|\sigma_1^-\eta\sigma_1^+|G\rangle + \langle G|\sigma_2^-\eta\sigma_1^+|G\rangle + ...\right] \\ &= \frac{1}{\sqrt{N}}\eta \\ \langle\Psi_\mathrm{A}|H_\mathrm{L}|G\rangle &= \frac{1}{\sqrt{N}}\langle G|(\sqrt{N-1}\sigma_1^- - S_2^-)\eta(\sigma_1^+ + \sigma_1^-)|G\rangle \\ &= \frac{1}{\sqrt{N}}\left[\langle G|\sqrt{N-1}\sigma_1^-\eta\sigma_1^+|G\rangle + ...\right] \\ &= \sqrt{1-\frac{1}{N}}\eta \end{aligned} \tag{72}$$

In order to transform these amplitudes to probabilities we simply have to square the results. This means, that the probability to go into a dark state increases and to go into a bright state decreases when increasing the total number of atoms N. In order to capture this effect even a mean-field approach suffices, as our hamiltonian necessary for explanation of this effect does not induce higher order operator products when observing time evolution of individual operators.

This is also supported by a significantly higher antenna gain in simulations when including coupling and multiple excitations again.

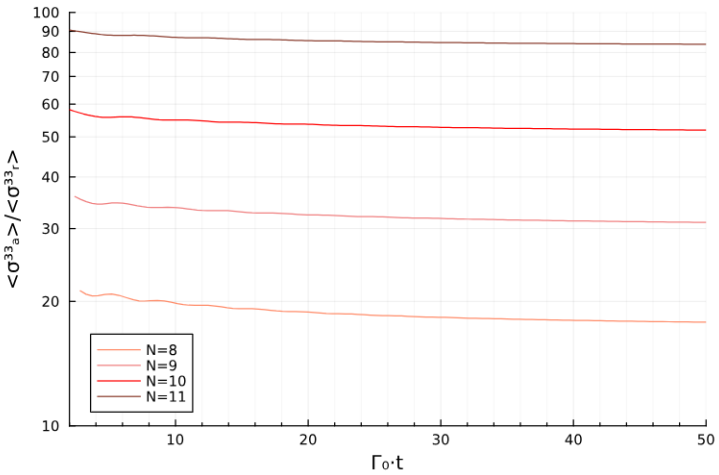

Figure 40: Time evolution of the antenna gain for different ring sizes, while keeping the inter-atomic spacing constant using mean-field. The gain scales related to equation 72, i.e. the gain increases with N quite significantly.

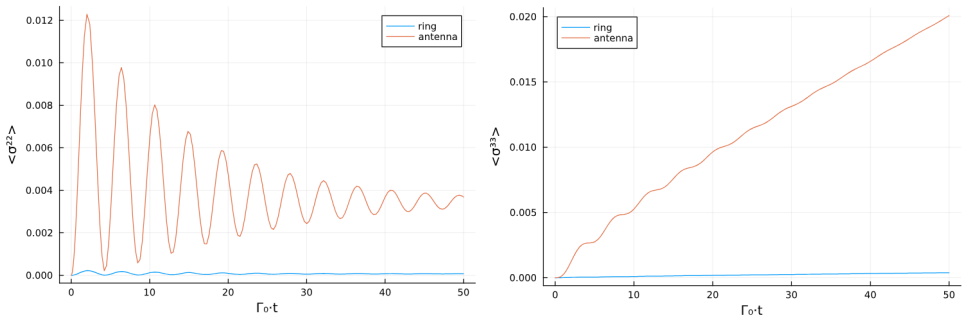

Figure 43: Time evolution of the population in the second and third energy level for the case where only the antenna unit in the center of the ring is irradiated with $\eta = 0.1\Gamma_0$ using mean-field. The fraction between excited state population in the antenna and the ring is distinctly larger than in the fully irradiated case, thus causing huge transfer into the target state $\langle \sigma_a^{33} \rangle$.

6 Conclusions

After recapping two-level systems, dipole-dipole interactions and treating the fundamental equations, we introduced the concept of cumulants and the cumulant expansion as a generalization of the mean field method.
We used it as an approximation method to express higher order through lower order expectation values and discovered its validity and efficiency.
Focusing on inter-atomic distances of $d \approx 0.05\lambda_0 - 1.0\lambda_0$ we found excellent performance with NCBE's of about 10^{-2} and less even for the lowest order in dense quantum systems of different geometries.
We investigated how this approximation relies on geometric quantities and explored operator time evolution for different quantum optical emitter arrays.

Furthermore, we could show that it is not just useful for approximating dynamics but for sensing for parameter regimes of interest. When comparing different orders, one can sense, for example, in driven systems for the parameters that cause a fine balance between well observable dynamics and the occurrence of quantum effects, which could certainly be put to use in experiments.
In a similar shape one can utilize, that the first order cumulant expansion yields results under consideration classical, giving access to comparisons between a classical and a quantum treatment of problems.

To get more insight into the cumulant expansion, it was performed analytically. We found, that at least for the case of the two-dipoles the cumulant orders behave similar to a taylor series expansion. Thus the first order is the leading order determining the envelope and it shares the same boundaries as any further expansion. Higher orders then modify the result to take quantum effects, i.e. coupling between emitters causing super- and subradiant states, into account. So one could reasonably argue, that ever higher orders will have lower impact on the overall dynamics, which would further motivate its use for large operator product averages.

Finally we concluded with a demonstration of the extreme computational efficiency on the example of a ring with a central impurity, generating results for systems consisting of ten atoms within seconds and we derived interesting quantum phenomena even when using mean field.

Overall the cumulant expansion as a generalized mean field method turned out to be a highly efficient and in the checked parameter regimes valid approximation and does suffer little from increasing system size.
However it is important to point out, that having significantly lower spacing between the atoms than their transition wavelength will most likely cause straight up wrong results, so it is definitely not suited e.g. when looking into microwave transitions in very dense atom arrays.

Cumulants are relevant in so much more topics than just quantum optics like condensed matter physics, fluid dynamics and even in finance and economy to capture price fluctuations and volatility. Having a valid tool to approximate them, so they can be used in realistic settings with our currently available computational power, is obviously of great use. I hope i could contribute to showing the validity of this method, motivate its use and maybe even expand the scope of use.

References

[1] Richard Tobin (1990). "Ancient Perspective and Euclid's Optics", Journal of the Warburg and Courtauld Institutes, Volume 53, Number 1

[2] Ling-An Wu, Gui Lu Long, Qihuang Gong, Guang-Can Guo, "Optics in Ancient China", AAPPS Bulletin, 2015, Vol 25, Issue 4, p6

[3] Bohr, N. Der Bau der Atome und die physikalischen und chemischen Eigenschaften der Elemente. Z. Physik 9, 1–67 (1922). https://doi.org/10.1007/BF01326955

[4] M.Sc. Verena Scheil (2022). "Exciton Dynamics in Coupled Nano-Rings of Dipolar Quantum Emitters", master thesis, institute for theoretical physics, Innsbruck

[5] D. Plankensteiner, C. Hotter, and H. Ritsch, QuantumCumulants.jl: "A Julia framework for generalized meanfield equations in open quantum systems", Quantum 6, 617 (2022)

[6] G.C.Wick (1950). "The Evaluation of the Collision Matrix", Physical Review. Band 80, Nr.2, P.268-272, doi:10.1103/PhysRev.80.268

[7] Ryogo Kubo. J. Phys. Soc. Jpn. 17, 1100-1120 (1962)

[8] "Documentation of QuantumCumulants.jl". https://qojulia.github.io/ QuantumCumulants.jl/ stable/ (Accessed: November 23, 2023).

[9] Dr. Laurin Ostermann (2016). "Collective Radiation of Coupled Atomic Dipoles and the Precise Measurement of Time", Doctoral thesis, institute for theoretical physics, Innsbruck

[10] Dr. Christoph Hotter (2018). "Superradiant Cooling, Trapping and Lasing of Dipole-Interacting Clock Atoms", P.2, master thesis, institute for theoretical physics, Innsbruck

[11] Sung-Hyuk Cha (2007). "Comprehensive Survey on Distance/Similarity Measures between Probability Density Functions", International journal of mathematical models and methods in applied sciences, Issue 4, Volume 1 [P. 300 - 307]

[12] M. Moreno-Cardoner, R. Holzinger, H. Ritsch (2022). "Efficient nano-photonic antennas based on dark states in quantum emitter rings". DOI: https://doi.org/10.1364/OE.437396

[13] L. Ostermann, H. Zoubi, H. Ritsch, "Cascaded collective decay in regular arrays of cold trapped atoms", 5 (2012). URL https://scholar.google.com/scholar?hl=de&as_sdt=0,5&q=cascaded +collective+decay+ostermann&btnG=

[14] P. Sowler-Wright, K. B. Arnardóttir, P. Kirton, B. W. Lovett, J. Keeling, "Determining the validity of cumulant expansions for central spin models", DOI: 10.1103/PhysRevResearch.5.033148

[15] M. Moreno-Cardoner, R. Holzinger, H. Ritsch, "Efficient nano-photonic antennas based on dark states in quantum emitter rings", DOI: https://doi.org/10.1364/OE.437396

universität innsbruck

Eidesstattliche Erklärung

Ich erkläre hiermit an Eides statt durch meine eigenhändige Unterschrift, dass ich die vorliegende Arbeit selbständig verfasst und keine anderen als die angegebenen Quellen und Hilfsmittel verwendet habe. Alle Stellen, die wörtlich oder inhaltlich den angegebenen Quellen entnommen wurden, sind als solche kenntlich gemacht.

Die vorliegende Arbeit wurde bisher in gleicher oder ähnlicher Form noch nicht als Magister-/Master-/Dipolomarbeit/Dissertation eingereicht.

23.2.2024	
Datum	Unterschrift